

DEPLOYMENT AND ON-ORBIT SHAPE MODIFICATIONS FOR A LARGE  
SPACE TELESCOPE USING MAGNETOSTRICTION

BY

MARIE-CAROLINE CORBINEAU

THESIS

Submitted in partial fulfillment of the requirements  
for the degree of Master of Science in Aerospace Engineering  
in the Graduate College of the  
University of Illinois at Urbana-Champaign, 2016

Urbana, Illinois

Advisor:

Professor Victoria L. Coverstone

## ABSTRACT

The Hubble Space Telescope, with its 2.4-m primary mirror, enabled notable scientific progress and discoveries, like for instance the acceleration of the expansion of the universe. Twenty-six years later, NASA is about the launch the next generation of space telescopes, namely the James Webb Space Telescope, with a diameter of 6.5 m. However the primary mirrors' limited size reduces the performance and thus possible scientific outcome of space telescope missions and the astronomers' desire for larger apertures will surely outstrip the ability of rocket fairings to accommodate these larger apertures. In response to the desire for larger mirrors, deployable mirrors are the logical choice.

The APERTURE mission presents a feasible approach toward the reality of deployable diffraction-limited ultraviolet-visible (UV-Vis) mirrors of 16-m diameter or larger. APERTURE uses a membrane mirror that will be folded like an umbrella and then deployed in space. Thanks to a magnetic smart material coating and a magnetic write head, post deployment corrections will be applied to the surface figure. The feasibility study of the concept has been done in the context of a NIAC Phase I study which is the result of a collaboration between Northwestern University and the University of Illinois at Urbana-Champaign. A video of the concept has been produced for more clarity. The design and analysis of the folded shape have been carried out to check that the telescope can be effectively stored in a Delta IV Heavy rocket fairing. Then the deployment of the primary mirror has been investigated and two different mechanisms have been selected. The feasibility of post-deployment shape corrections has been studied and the impact of different key design parameters has been computed as a first step towards design optimization. A preliminary design has been obtained which also uses the results of the work carried out at Northwestern University. Finally, a work plan and test campaign have been produced for the potential Phase II of the project.

## ACKNOWLEDGEMENTS

I would like to express profound gratitude to my advisor Professor Victoria L. Coverstone for trusting me and giving me the opportunity to be part of this project. I really appreciate the supportive attitude that she kept throughout my thesis and all the good pieces of advice that she provided me with.

I would like to give special thanks to the members of the research team at UIUC: Alexander Case, Christopher Lorenz, Guanyang Luo, Brandon Murchison, Jeffrey Pekosh and Jose Sepulveda. They all put a lot of work and energy in this project.

I greatly appreciate the guidance from, and interaction with the PI of this project, Professor Melville P. Ulmer. I would like to particularly thank him for giving me responsibilities in this project.

Thanks also to our other collaborators at Northwestern University Professor Yip-Wah Chung, Professor Jian Cao, Andreas Schneider, Xueting Yan and Shi Ye.

This work was supported by a NASA NIAC grant number NNX15AL89G. I gratefully recognize many of the people who have given us input and support: Dr. G. Pareschi who introduced us to Dr. C. Joshi who introduced us to MSM films and their applications; Drs. X. Wang, Y. Yao, C. Liu who carried out MSM film coatings and the related measurements and modeling of deformation on glass; Drs. C. S. Arnold and D. Pappas for input on magnetic write heads, and Dr. S. Padula regarding SMAs.

TABLE OF CONTENTS

**1 INTRODUCTION . . . . . 1**

1.1 Description of the APERTURE Concept . . . . . 1

1.2 Need for the Concept . . . . . 2

1.3 Funding Agency and Organization . . . . . 3

1.4 Potential Mission and Benefits to NASA . . . . . 4

1.5 Phase I Goals, Objectives and Tasks . . . . . 5

**2 DEPLOYMENT STUDY . . . . . 9**

2.1 Rocket Fairing and Constraints for the Stowed Configuration . . . . . 9

2.2 Design of the Folded Membrane . . . . . 10

2.3 Analysis of the Shape . . . . . 12

2.4 Determination of a Condition before Micro-Yield . . . . . 14

2.4.1 Equations and Background . . . . . 14

2.4.2 Results . . . . . 16

2.5 Selection of Two Deployment Mechanisms . . . . . 18

2.5.1 The Flexible Precision Reflector (FPR) . . . . . 18

2.5.2 Self-Deployable Shell Reflector . . . . . 19

2.5.3 Summary . . . . . 20

**3 OPERATIONS AND CHARACTERISTICS OF THE POST DE-  
PLOYMENT SHAPE CORRECTING SYSTEM . . . . . 21**

3.1 Identification of a Key Parameter to Evaluate the Feasibility of Post  
Deployment Corrections . . . . . 21

3.2 Description of the Algorithm Used for the Computation of the Time  
Needed to Correct the Mirror . . . . . 21

3.3 Baseline Values of the Parameters . . . . . 22

3.4 Results . . . . . 25

3.4.1 Impact of Different Parameters . . . . . 25

3.4.2 Summary . . . . . 32

<b>4</b>	<b>PRELIMINARY APERTURE DESIGN . . . . .</b>	<b>36</b>
4.1	Magnetic Smart Material and Substrate . . . . .	36
4.2	Magnetic Write-Head . . . . .	36
4.3	Stowed Configuration and Deployment Mechanism . . . . .	37
4.4	Post-Deployment Figure Assessment and Feedback . . . . .	38
4.5	Operations of the In-Space Shape Correcting System . . . . .	38
<b>5</b>	<b>CONCLUSION . . . . .</b>	<b>39</b>
5.1	Future Work . . . . .	39
5.1.1	Concept Verification Testing . . . . .	39
5.1.2	Tall Poles for Phase II . . . . .	42
5.1.3	Work Plan for Phase II . . . . .	43
<b>6</b>	<b>PUBLICATIONS AND CONFERENCES . . . . .</b>	<b>49</b>
	<b>REFERENCES . . . . .</b>	<b>50</b>

## CHAPTER 1 INTRODUCTION

### 1.1. Description of the APERTURE Concept

Described within this thesis are the results that establish the APERTURE mission concept as a feasible approach toward the reality of deployable diffraction-limited ultraviolet-visible (UV-Vis) mirrors of 16-m diameter or larger. APERTURE, which stands for "A Precise Extremely large Reflective space Telescope Using Reconfigurable Elements", uses a Magnetic Smart Material (MSM) to apply figure corrections to extremely large ( $\geq 16$ -m) deployable reflective optics. The first step of the deployment will utilize an umbrella-like structure to achieve a parabolic shape for the optics. The inside of the umbrella will be the reflective surface, while the outside will be coated in MSM. A magnetic write head will move to different locations on the MSM coated side to manipulate the MSM, changing the shape of the optics and eliminating any deviation from the desired final shape. Figure 1.1 depicts the concept of APERTURE: the write head (in dark brown color) moves along the curved arm, while the curved arm rotates about the center axis.



Figure 1.1: APERTURE concept. For simplicity only one write head is shown.



Figure 1.2: The QR code leads to an animation depicting the concept <https://www.youtube.com/watch?v=4j-Elbjvh78&feature=youtu.be>

## 1.2. Need for the Concept

The desire for larger space telescopes is ever present. The UV-Vis Hubble Space Telescope (HST) and the near-infrared (NIR) James Webb Space Telescope (JWST) have a diameter of 2.4 m and 6.5 m respectively. The Advanced Technology Large-Aperture Space Telescope (ATLAS-T) concept has a desired maximum diameter of 16 m [1] and requires the 10-m baseline fairing of the now canceled Ares V heavy lift vehicle [2]. Therefore, even if rocket fairings are made larger, the astronomers' desire for larger apertures will surely outstrip the ability of rocket fairings to accommodate these larger apertures.

In response to the desire for larger mirrors, deployable mirrors are the logical choice. Within this category there are segmented mirrors, e.g. JWST, and a preliminary conservative approach of scaling up JWST by unfolding rigid segments yields approximately a 12-m diameter design [3]. Conversely, for deployable membrane optics, the limiting diameter is more than 16 m. However, the problem with any membrane-like mirror such as the Tracking and Data Relay Satellites (TDRS) [4] or the AstroMesh design [5], is that they have yet to achieve a better shape than the figure accuracy acceptable for S, Ku and Ka-band wavelengths (respectively  $\sim 150$  mm,  $\sim 20$  mm,  $\sim 11$  mm). If one assumes a Strehl ratio of 90% (which is a measure of the quality of the optical image), then the Ka-band wavelength corresponds to a figure Root Mean Square (RMS) error of about  $11$  mm/20. Since APERTURE is meant to be used for UV-Vis observation, a similar Strehl ratio would lead to a RMS of  $400$  nm/20 (or better for the deep UV). Therefore if a deployed membrane mirror is to be employed, then post-deployment corrections will need to be applied within the context of current

designs.

The general concept of membrane and deployable mirrors associated with electrostatic or piezoelectric control has been studied in the past. A big disadvantage is that wires must be attached to every point on the mirror for which actuator control is needed, and so far the ability to provide post deployment figure corrections to the level of  $\lambda/20$  in the visible for membrane mirrors has eluded the space community. Previous work has been done using polyvinylidene fluoride (PVDF) actuators for surface control on a flexible Kapton reflector by Jeffrey R. Hill, et al. [6]. Their experiment concluded that a feasible RMS surface error between  $\sim 100 \mu\text{m}$  and  $400 \mu\text{m}$  is obtainable depending on the initial configuration of the reflector. While a surface error of this scale is accurate enough for long ( $\sim 1 \text{ mm}$ ) wavelength reflectors, a reflector operating in the UV wavelength range requires a surface error of at most 10 nm. Therefore, a UV-Vis space reflector requires an alternate method of post deployment correction from piezoelectric actuators. What is new about our approach is that it uses moving magnetic write heads to modify the mirror figure *without attachment* to the mirror.

There has also been recent excitement generated by a concept funded by DARPA [7]. The DARPA approach uses diffraction from the membrane surface as illustrated on Figure 1.3, whereas our concept uses the more classic concept of reflection from the mirror surface. Using the proposed method, high quality images could be made from the extremely large optics, opening up a wide variety of opportunities for new discoveries. This will be a game changing technology for astronomy, as astronomy is always light limited.

### 1.3. Funding Agency and Organization

This work was supported by a Phase I NASA Innovative Advanced Concept (NIAC) grant number NNX15AL89G. This project is based on a collaboration between Northwestern University (NU) and the University of Illinois at Urbana-Champaign (UIUC). The work has been divided between the two universities; the team at NU was in charge

---

<sup>1</sup>[www.ubergizmo.com/2013/12/moire-folding-telescope-from-darpa/](http://www.ubergizmo.com/2013/12/moire-folding-telescope-from-darpa/)



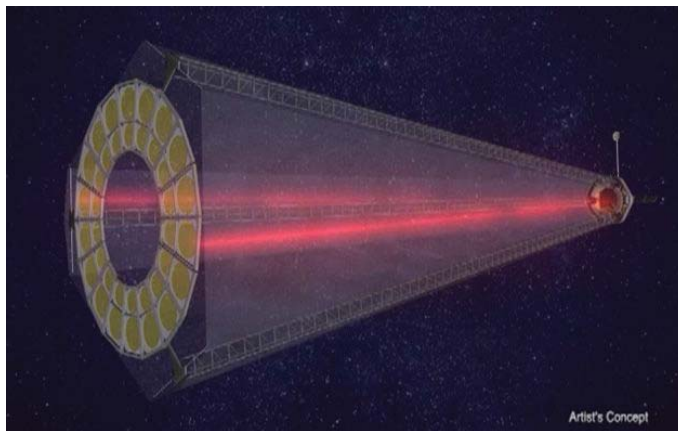


Figure 1.3: MOIRE diffraction telescope concept (DARPA project) <sup>1</sup>

of the magnetostriction and magnetic smart material aspects of the project, while the team at UIUC studied the telescope deployment and operation feasibility of the post deployment correction system. The results obtained at NU are not detailed in this report but they are summarized in chapter 4 which deals with the preliminary design.

#### 1.4. Potential Mission and Benefits to NASA

In contrast to using magnetostriction, all current space mirrors rely on the piezoelectric effect which then requires that actuators be attached to the mirror and that wires need to be attached to the actuators. The piezoelectric approach is the baseline for the Advanced Technology Large-Aperture Space Telescope (ATLAS-T) mission and the APERTURE concept presents great potential benefits to this future mission. A major benefit of our approach of using a flexible mirror rather than many combined rigid segments, is that the design can be expanded well beyond the current 16-m diameter (the proposed maximum diameter) of ATLAS-T [1]. Indeed, provided that the membrane is thin enough, we can apply our umbrella design to larger diameters (see 2.2). Larger mirrors with commensurate figure quality open up a larger discovery space. Also, the maturing of the technology proposed here would lead, by extension, to even more technological challenges such as the Terrestrial Planet Finder[8]. In addition, the ATLAS-T concept, which required the 10-m baseline fairing of the now canceled Ares V heavy lift vehicle [2], needs the future modified Space Launch System (SLS) while it is proved in the Phase I study that a membrane mirror can fit into the

existing Delta IV Heavy rocket fairing without producing structural micro-yield.

The overall goal of Phase I and Phase II is to produce a proof that the technology concept underlying APERTURE has enough merit to follow through with aggressive funding to bring the idea to TRL 6. Phase I was entirely a paper study to design experiments and extensive (beyond those in Phase I) computations to be carried out in Phase II. The Phase I also helped the team identify many of the problems the APERTURE concept faces. The resulting tall pole list is given in section 5.1.2. As an aside, it should be noted that although the focus of this project is the comparison to the NASA ATLAS-T astronomical telescope project, NASA's Earth Observing Office is equally interested in large aperture telescopes.

#### 1.5. Phase I Goals, Objectives and Tasks

To develop this technology, several aspects were explored via a literature search, calculations, and simulations:

- Determine materials that are both flexible enough to be folded up and yet rigid enough to maintain this figure with fine post deployment adjustments.
- Determine the best magnetic material to coat the mirror, which is flexible and does not distort the figure beyond the possible correction range.
- Determine a design for the write head system that has a strong enough magnetic field to affect the desired changes on the required length scales across the mirror.
- Determine an approach to vary the magnetic field strength and direction, e.g., two permanent pole magnets whose orientation and distance from the mirror change the magnet field, versus an electromagnet which varies the magnetic field strength by changing the current.
- Determine how to coat large monolithic membranes with the requisite material, or how to stitch together segments that are small enough to coat easily.
- Determine how to characterize the mirror figure in orbit.

- Determine how to ensure that the figure can hold its shape for times longer than the time required to bring the figure into shape.
- Select potential deployment mechanisms that can lead to an accurate post deployment shape which could then be corrected using magnetic write heads.

Given the above requirements, major tasks were carried out via literature search, calculations, and simulations, and were organized as follows:

**Task 1: Select a set of materials, characterize them, and define thicknesses necessary for a test in Phase II**

Major Task 1 was led by Ulmer (overall organization plus direct supervision for the ray tracing simulations) along with input from key personnel, Chung (Materials with a focus on magnetic properties of them) and Cao (Mechanical Engineering and deflection vs stress).

Task 1.1: Find a polymer thick enough to not be too floppy but thin enough to be correctable over the smallest length scales.

Task 1.2: Find a magnetic hard material thick enough to hold in the field, but thin enough to be flexible.

Task 1.3: Find a MSM material that is thin enough to be flexible but strong enough to make the shape changes needed over the requisite length scale.

Task 1.4: Determine an adhesion process among all the layers.

Task 1.5: Evaluate Coefficient of Thermal Expansion (CTE) issues of survivability during transport and launch.

Task 1.6: Determine the length scale for figure correction need to be made via ray tracing and feed back this information to the properties of the reflecting layer, the polymer, the MSM, and magnetic hard material.

Task 1.7: Determine if the MSM can also be a magnetic hard material, and if so, what should it be.

Task 1.8: Match the annealing temperature to substrate such that annealing, if necessary, will not damage the substrate.

Task 1.9: Determine the extent, if any, that out-gassing will affect the shape and or

surface once deployed in space.

**Task 2: Develop a process for large scale replication of 200 m<sup>2</sup> or more reflective surface**

If a convincingly affordable design which matches with the MSM concept cannot be devised, the other parts of the design will not matter. Feedback between the substrate fabrication techniques and the deployment was considered. Major Task 1 was joint with the personnel at NU (Ulmer, replication; Chug, materials), and UIUC (Coverstone, deployment).

**Task 3: Produce a preliminary design of the stowage and deployment**

Stowage and deployment designs need to take into account both how each segment or monolithic membrane is formed, as well as the materials used. A preliminary design was carried out in Phase I. Major Tasks 3-4 were primarily carried out by UIUC: Coverstone was the key personnel, with input on deflections and write head capabilities from Chung and Cao.

**Task 4: Produce a preliminary design of the magnetic write head system**

The magnetic write head, and how it is to be moved around, requires a preliminary design and a preliminary determination of the requirements of the write head coupled with the deployment design. The deployment depends on the design of the magnetic write head because if, for instance, the magnet is moved around on some kind of wire, the deployment of the wire can be critical. This item is an engineering challenge as it can cause limitation on the overall design. In the case of the wire, for example, the use of jets would be inappropriate because of contamination and because the design would have an expendable component which is undesirable for long term operability. This task also covers the issue of the placement of the magnet relative to the surface.

**Task 5: Synthesize an overall preliminary design**

Major tasks 5 and 6 were performed by all personnel.

## Task 6: Reporting and meeting

Progress reports were written every two months, as well as a final report for Phase I at the end of month 9. Additionally, PI Melville P. Ulmer attended the two required program meetings, namely the two-day NIAC orientation meeting and the three-day NIAC symposium.

The schedule of the above mentioned tasks and their respective milestones are presented on Figure 1.4.

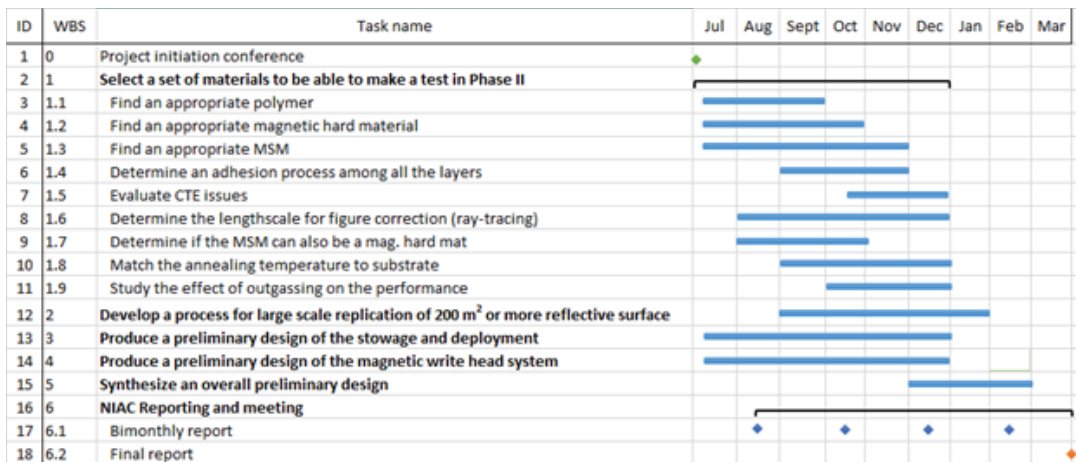


Figure 1.4: Schedule for Phase I

## CHAPTER 2 DEPLOYMENT STUDY

### 2.1. Rocket Fairing and Constraints for the Stowed Configuration

APERTURE’s deployment design assumes the utilization of a Delta IV Heavy rocket which can carry a payload with a diameter up to 4.6 m and a height less than 17 m. For simplicity, only solid monolithic designs will be considered for the secondary mirror and, given the dimensions of the rocket fairing, its diameter is constrained to be less than 4.6 m. Initially, both segmented and monolithic approaches were considered for the deployment study. Segmented approaches, are usually associated with piezo or mechanical actuators that are responsible for aligning the segments after deployment. This is in contradiction with the original purpose of APERTURE which is to avoid the utilization of piezo-actuators. Moreover, JWST uses 18 hexagonal segments with two foldable panels but for primary mirrors as large as APERTURE’s, segments of the size used for JWST would not fit.

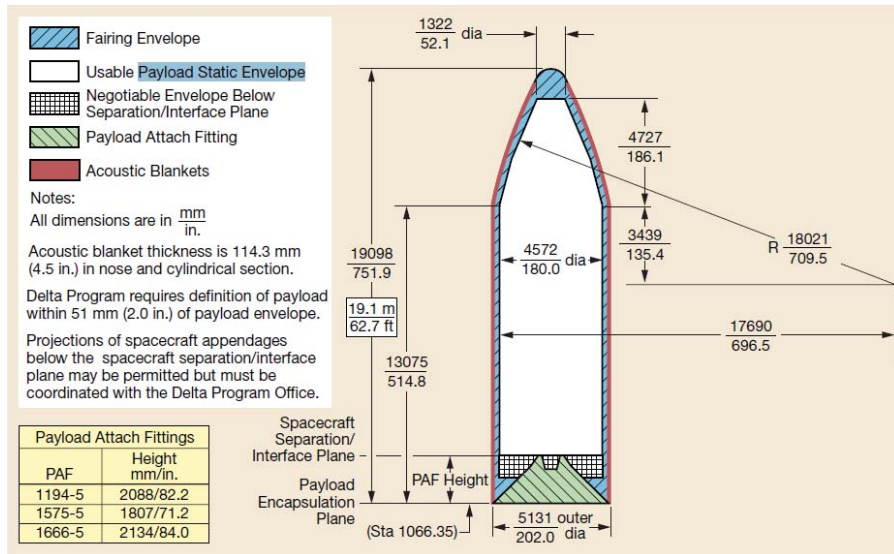


Figure 2.1: Payload Static Envelope, 5-m diam by 19.1-m Composite Fairing, Delta IV Heavy [9]

Given the dimensions of the desired rocket fairing, if the mirror is monolithic then it needs to be flexible. Moreover, the thinner a membrane is, the easier it is to make corrections with a magnetic write head. However, if the membrane is too thin, it

would not be able to hold its parabolic shape. Therefore, some stiffeners are needed. Another parameter that needs to be taken into account in the calculation of the thickness of the membrane is its extreme susceptibility to micro-yield (microscopic plastic deformation). It is necessary to make sure that the membrane can be folded within the rocket fairing without being damaged.

## 2.2. Design of the Folded Membrane

The first shape that has been considered is the umbrella design. This shape has been studied by Enders et al. [10], however, there is a limitation due to the way the section is generated since it is based on circles, and for large apertures this strategy is not applicable, as shown on Figure 2.2. In this report we present a variation of the method described by Enders et al.; instead of generating the section using circles we use Equation 2.1 and Equation 2.2 where  $2p$  is the number of petals and  $r_0 + \rho$  is the maximal radius of the stowed membrane.

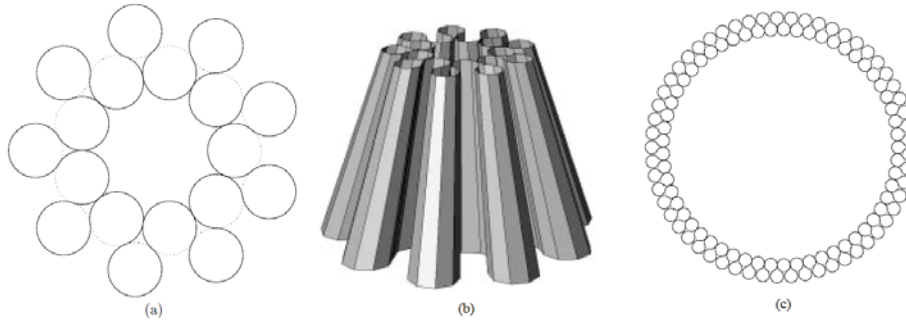


Figure 2.2: (a) Section using circular shape, (b) corresponding 3D umbrella shape, (c) failure of the umbrella design

$$\theta = t + \cos^4(pt) \quad (2.1)$$

$$r = r_0 + \rho \cos^4(pt) \quad (2.2)$$

The corresponding results for 6.5-m and 16-m diameter mirrors are displayed on Figure 2.3; the diameter of the 16-m diameter folded mirror is 3.9 m which corresponds to a margin of 15% with respect to the Delta IV Heavy rocket fairing inner diameter. In order to determine the free parameters of Equation 2.1 and Equation 2.2, the

maximal curvature of the section has been minimized according to the three following constraints:

- the number of petals is an integer :  $p = \frac{k}{2}, k \in \mathbb{N}$
- the diameter is known and the perimeter is fixed  $L = \pi D$
- the stowed membrane must fit into the rocket :  $r_0 + \rho \leq R_{Rocket}$

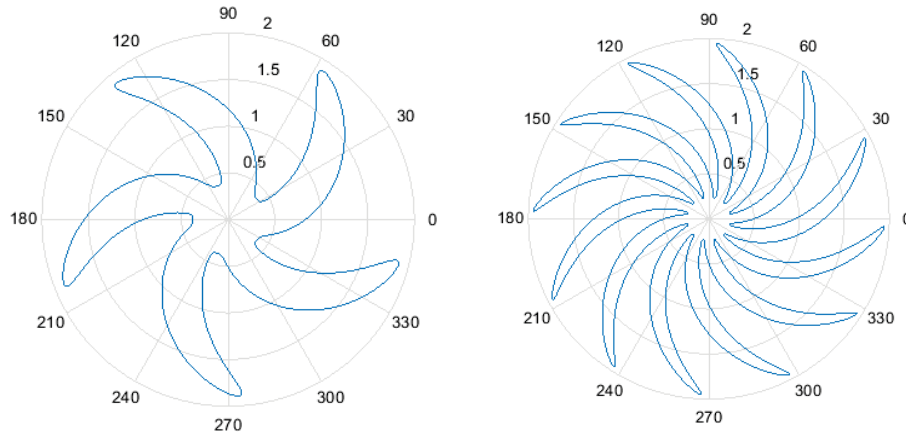


Figure 2.3: Top section of an umbrella-like folded mirror (a) 6.5-m diameter, (b) 16-m diameter.

First we need to express the derivatives that will be used to compute the circumference and the curvature (see Equations 2.3, 2.4, 2.5, 2.6). The circumference is calculated in Equation 2.7, and the curvature is obtained thanks to Equation 2.8.

$$\frac{d\theta}{dt} = 1 - 4p \sin(pt) \cos^3(pt) \quad (2.3)$$

$$\frac{dr}{dt} = -4pp \sin(pt) \cos^3(pt) \quad (2.4)$$

$$r' = \frac{dr}{d\theta} = \frac{dr}{dt} \frac{dt}{d\theta} \quad (2.5)$$

$$r'' = \frac{d}{d\theta} \left( \frac{dr}{d\theta} \right) = \frac{4p^2 \rho \cos^2(pt) (1 - 2\cos(2pt))}{(1 - 4p \sin(pt) \cos^3(pt))^3} \quad (2.6)$$

$$L = \int_{\theta_1}^{\theta_2} \sqrt{\left(\frac{dr}{d\theta}\right)^2 + r(\theta)^2} d\theta \quad (2.7)$$



$$\gamma(\theta) = \frac{r^2 + 2r'^2 - rr''}{(r^2 + r'^2)^{\frac{3}{2}}} \quad (2.8)$$

### 2.3. Analysis of the Shape

Results for different values of the mirror's diameter are shown on Figure 2.4 ( $R_{rocket}$  was set equal to 2.1 m but the resulting diameter of the folded membrane can be smaller). The number of petals increases linearly with the diameter of the mirror (Figure 2.4), while the minimal radius of curvature decreases and can be approximated by a power function of the mirror diameter (Figure 2.5). Some points of the section, on the outer and inner edges, exhibit very low radii of curvature, leading locally to a greater probability of micro-yield; therefore an analysis of the material's properties is necessary to determine if it can be folded according to those high values of the curvature.

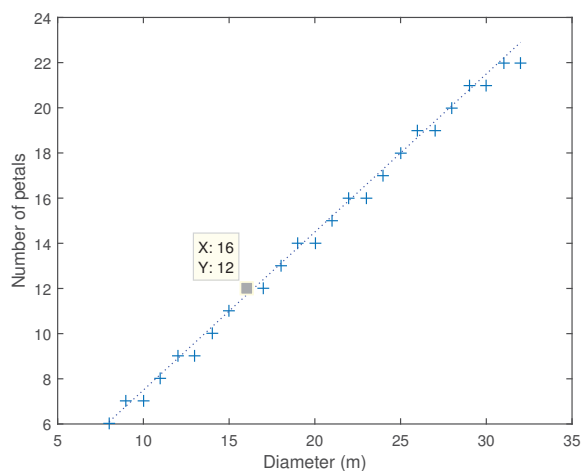


Figure 2.4: Number of petals as a function of the mirror's diameter.

The corresponding 3D shape has been obtained for a cone: Figure 2.6 shows the resulting umbrella shape for a 6.5-m and a 16-m diameter mirror; similar work can be done for a parabola. The final shape has been obtained taking the focal length equal to the diameter:  $F/D = 1$ . Moreover, the inner hole can be calculated by scaling up the JWST design:  $D_{min}/D_{max} = 0.203$  which would give  $D_{min} = 3.2$  m for the 16-m diameter mirror. However, for the 3D shape, the minimal radius of curvature is found

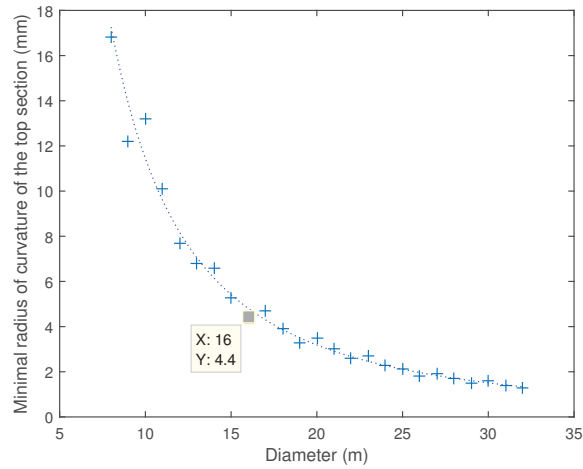


Figure 2.5: Minimal radius of curvature on the top section for different values of the mirror's diameter.

at the base, not on the top section. Thus, in order to decrease the risk of micro-yield, one can increase the size of the inner hole, although a portion of the reflective area would be lost. By taking  $D_{min}/D_{max} = 0.28$ , the inner hole is approximately equal to the maximal size of the secondary mirror,  $D_{min} = 4.5$  m. Using this ratio, the collecting surface area represents about 92% of the total surface while, using the ratio of JWST, 96% of the reflecting side would be used. However, the minimal radius of curvature of the lower section of the umbrella is significantly improved, being equal to 1 mm for  $D_{min}/D_{max} = 0.28$ , against 0.5 mm when  $D_{min}/D_{max} = 0.203$ .

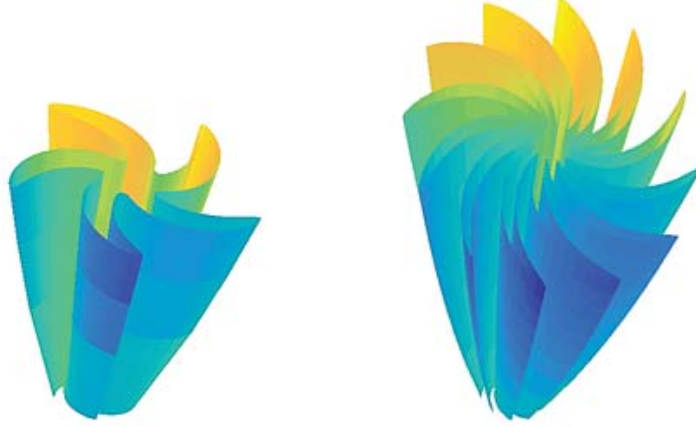


Figure 2.6: Umbrella-like folded mirror (a) 6.5-m diameter, (b) 16-m diameter (the colors are not meaningful, they are just used for visualization).

## 2.4. Determination of a Condition before Micro-Yield

### 2.4.1. Equations and Background

There is a minimal radius of curvature allowable before producing micro-yields in the structure; it depends on the materials that are used to make the membrane. The final composition of the membrane is not determined yet but preliminary results have been obtained for materials that are likely candidates. A similar calculation can be done once the composition of the membrane is known. The flexibility of a material, or allowable minimal radius of curvature, can be computed according to the analytic approach of Domber and Peterson [11]. The limit for the minimal allowable radius of curvature,  $R_F$ , is achieved when micro-yields appear in the material. Usually, the criterion of the elastic "0.2%" yield stress is chosen, but for optical components even small residual strains must be considered. The calculation of  $R_F$  is based on Equation 2.9.

$$\omega \approx \left( \frac{t}{2R_F} \frac{E}{H} \right)^{\frac{1}{n}} \frac{\widehat{D}^2}{4t} \quad (2.9)$$

Here the variable  $\omega$  is the allowable deflection,  $t$  is the thickness of the material,  $E$  is the Young's modulus of the material,  $H$  is the plasticity model constant,  $n$  is

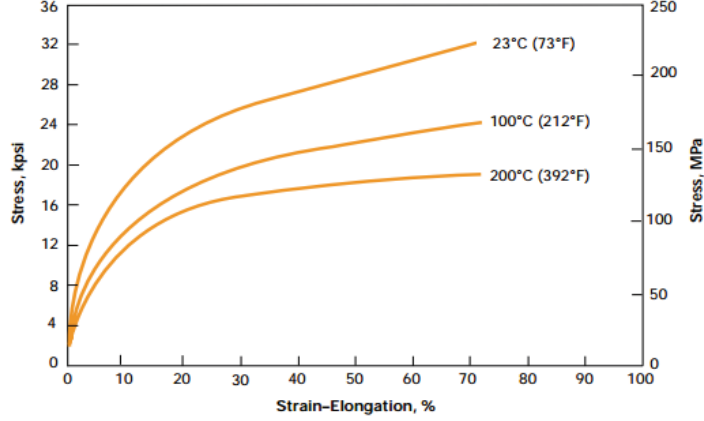


Figure 2.7: Strain-stress curves for Kapton®(courtesy of Dupont<sup>2</sup>) at different temperatures

the strain hardening exponent and  $\hat{D}$  is the length of the surface which is curved. For localized curvature (in the case of the umbrella-like deployment for instance),  $\hat{D}$  can be approximated by  $\hat{D} = 2\pi R_F$  [10]. The main hypothesis behind this formula is that, for very small deformations, the plastic term in the Ramberg-Osgood model (Equation 2.10) can be neglected with regards to the elastic term. Equation 2.9 then leads to Equation 2.11.

$$\epsilon = \frac{\sigma}{E} + \left(\frac{\sigma}{H}\right)^{\frac{1}{n}} \quad (2.10)$$

$$R_F \approx \left(\frac{\omega t}{\pi^2} \left(\frac{2H}{tE}\right)^{\frac{1}{n}}\right)^{\frac{n}{2n-1}} \quad (2.11)$$

The plastic parameter  $H$  and the exponent  $n$  can be found using the Ramberg-Osgood model for one-dimensional yield (Equation 2.10). The strain-stress curve of a material can be approximated by the model represented by Equation 2.10. For instance, a least-squares approximation, applied to the 23°C strain-stress curve for Kapton (Figure 2.7), leads to  $n_{Kapton} = 0.238$  and  $H_{Kapton} = 0.249$  GPa (see Figure 2.9). The same method is applied to Galfenol (see Figure 2.8 and Figure 2.10). The exponent  $n$  takes its value between 0 and 1, and the smaller  $n$  is, the more plastic the material is. For aluminum Al 2024-T3, the value for  $H$  and  $n$  have been found in [11] :  $H = 0.68$  GPa,  $n = 0.06$ .

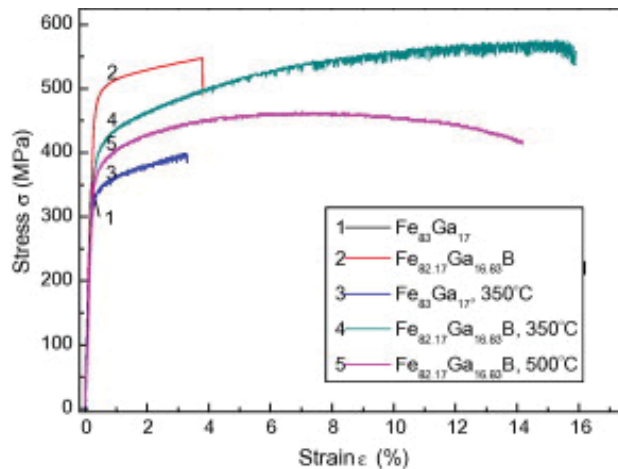


Figure 2.8: Strain-stress curves for Galfenol [12] at different temperatures

To compute  $R_F$  using Equation 2.11, a value for the deflection  $\omega$  must be chosen. Usually, the maximal deflection allowed for a mirror is expressed as a fraction of the shortest operating wavelength of the reflector [10]:

$$\omega_{max} \leq \alpha \lambda_{min}$$

For APERTURE,  $\lambda_{min}$  is taken to be 200 nm (UV). The value for  $\alpha$  will be determined during Phase II of the NIAC program, but 1/20 is thought to be a lower limit. Thus,  $\omega_{max} \leq 10nm$ . Nevertheless, APERTURE will get the advantage of post deployment corrections; hence, it is reasonable to take a higher value for the maximal deflection, say  $1\mu m$ . Figure 2.11 illustrates the impact of  $\omega_{max}$  and of the thickness on  $R_F$ .

#### 2.4.2. Results

The results obtained for three types of material are summarized in Table 2.1. Aluminum, which has a high reflectance for UV, is a candidate for the reflective material, Kapton may be used as a substrate, and Galfenol is a magnetostrictive material similar to Terfenol-D, but more pliable and less subject to delamination.

<sup>2</sup><http://www.dupont.com/content/dam/dupont/products-and-services/membranes-and-films/polyimide-films/documents/DEC-Kapton-summary-of-properties.pdf>

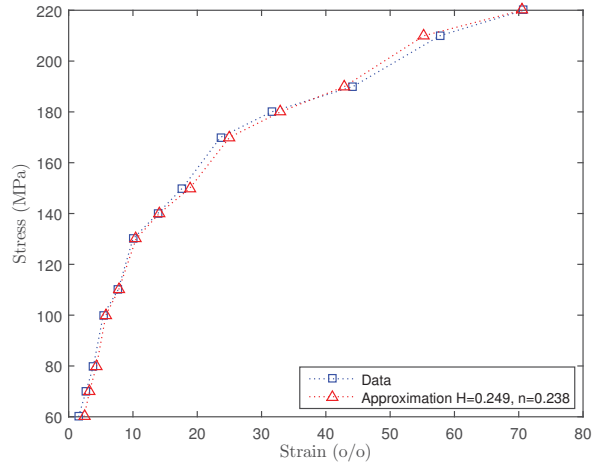


Figure 2.9: Strain-stress curve for Kapton (23° C), data and approximation

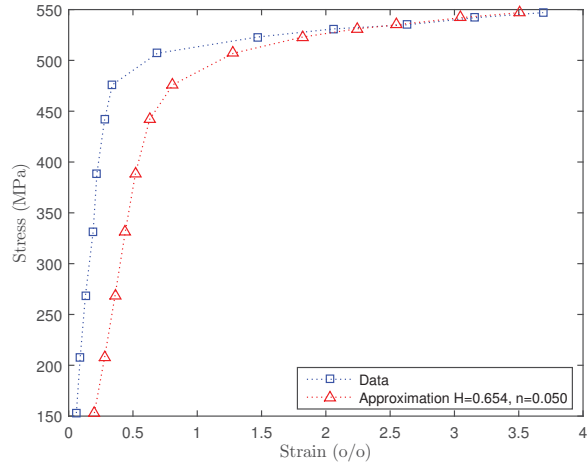


Figure 2.10: Strain-stress curve for Galfenol ( $Fe_{82.17}Ga_{16.83}B$ ), data and approximation

Table 2.1: Pliability, allowable radius of curvature before micro-yield, for different materials and various values of the thickness ( $\omega = 1\mu m$ )

Thickness ( $\mu m$ )	Al 2014-T6 (mm)	Kapton (mm)	Galfenol (mm)
10	1.2	1.7	1.2
20	2.6	4.8	2.4
25	3.3	6.6	3.1
50	6.9	18	6.3

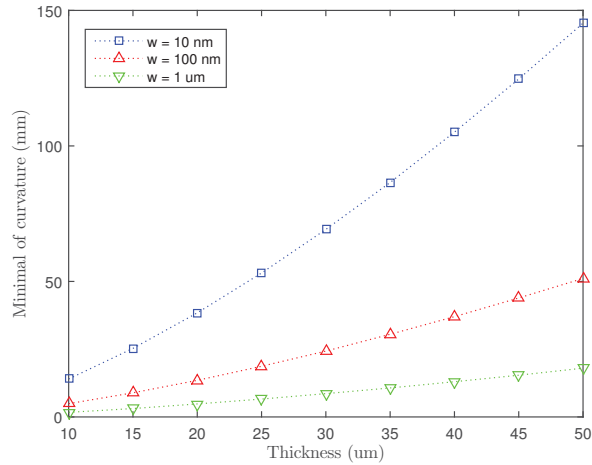


Figure 2.11: Radius of curvature before micro-yield for Kapton with different values of the deflection

## 2.5. Selection of Two Deployment Mechanisms

Now that the feasibility of stowing the mirror membrane in the Delta IV heavy fairing has been demonstrated, the deployment mechanism needs to be devised. The two main criteria that have been used to characterize the different strategies are the ability to stow the primary mirror into a Delta IV Heavy rocket fairing without damaging the surface, and the possibility of deploying the mirror into space while assuring that the final shape is precise enough to be corrected by applying the magnetic write head on the MSM. Other relevant parameters are the stowed volume efficiency, the stability, and the launch weight. Based on those criteria two types of deployment have been selected to carry out an experimental test campaign in a Phase II. Figure 2.12 shows a conceptual view of the flexible primary mirror deployment; a video of the full deployment is accessible online<sup>3</sup>.

### 2.5.1. The Flexible Precision Reflector (FPR)

The first design that has been selected is based on the use of a classic composite material combined with an elastic memory composite like  $\text{\textcircled{R}}\text{TEMBO}$ .  $\text{\textcircled{R}}\text{TEMBO}$  was created by Composite Development Technology (CTD) and was used by Harris Cor-

<sup>3</sup><https://www.youtube.com/watch?v=4j-Elbjvh78&feature=youtu.be>

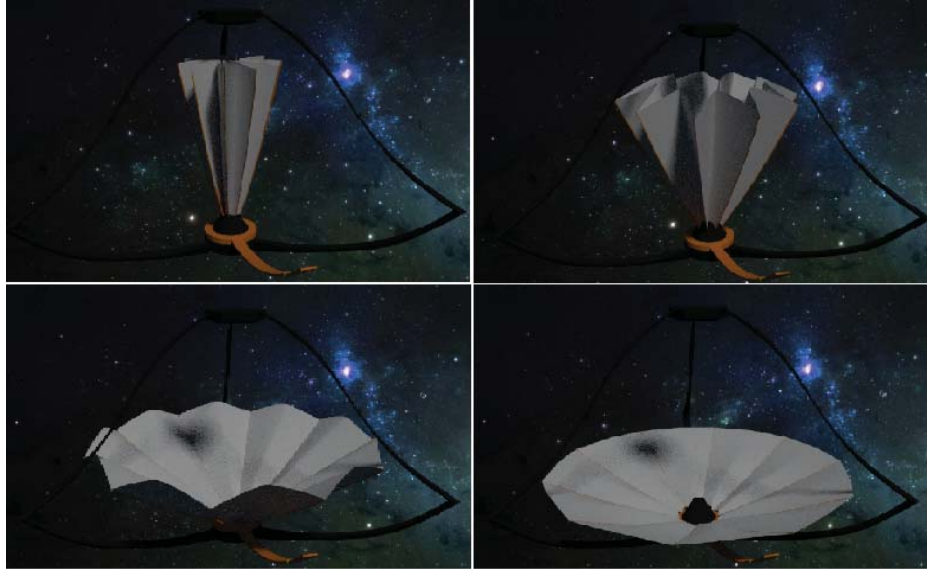


Figure 2.12: APERTURE deployment (conceptual view), see Figure 1.1 for the fully deployed telescope

poration to study the umbrella deployment of a Flexible Precision Reflector (FPR) [13]. The FPR can operate at radio frequencies (40 GHz, wavelength: 7.5 mm) and benefits from a very-low-packaged volume, a potential diameter of 25 m and a very low areal mass density. The reflector is deployed by heating the stiffeners, leading to a gradual, controlled and predictable mechanism (Figure 2.13).



Figure 2.13: Flexible precision reflector before and after deployment [13]

### 2.5.2. Self-Deployable Shell Reflector

An alternative to the umbrella design is the self-deployable shell reflector recently developed by Soykasap *et al.* [14]. The deployment of a 1.5-m diameter reflector is illustrated on Figure 2.14. The material used is a Carbon Fiber Reinforced Polymer



(CRFP). The size of the reflector is limited by the height of the rocket but a Delta IV Heavy rocket fairing would still allow a 17-m diameter primary mirror which is already a notable improvement compared to currently used space telescopes. The deployment of this reflector requires no additional external energy, but the sudden release of stored strain energy can create vibrations in the structure.



Figure 2.14: Deployment of the self-deployable shell reflector (duration: 1.4 s) [15]

### 2.5.3. Summary

Table 2.2 summarizes the main characteristics of the prototypes that have been manufactured according to the two designs described above. The RMS error values can be compared to the magnitude of the maximal deflection that one can obtain using MSM as studied by the team at NU. The CRFP may prove too stiff, but the FRP has quite a low Young's modulus, measured in tens of kPa [16].

Table 2.2: Characteristics of the two selected deployment designs

Design	Diameter	Thickness	Material	RMS error
Flexible Precision Reflector (FPR) [13]	0.9 m	152 $\mu m$	TEMBO® <sup>®</sup> , elastic memory composite	330 $\mu m$
Self-deployable flexible shell [14]	1.5 m	220-880 $\mu m$	CRFP, plain weave	420 $\mu m$

## CHAPTER 3 OPERATIONS AND CHARACTERISTICS OF THE POST DEPLOYMENT SHAPE CORRECTING SYSTEM

### 3.1. Identification of a Key Parameter to Evaluate the Feasibility of Post Deployment Corrections

In order to avoid the risks of having a fixed wire attached to a moving component, the magnetic write head will be wireless and will be powered by a battery which will be recharged on a charging station. The initial design of APERTURE, illustrated on Figure 1.1 (see also the animation referenced in section 1.1) includes only one magnetic write head moving on a single arm. However, this design will likely be modified given the size of the 16-m primary mirror; indeed, if the time during which the MSM holds its shape is shorter than the time needed to correct the shape using a single magnetic write head, then APERTURE would not be feasible. Thus, it is necessary to determine how many magnets are required to make post deployment corrections in a reasonable time. Other parameters like the size of the magnet's battery or the percentage of the spacecraft's main battery which is allocated to the magnetic write head can influence the duration of the correction process.

### 3.2. Description of the Algorithm Used for the Computation of the Time Needed to Correct the Mirror

To carry out this analysis, a worst-case scenario is chosen, assuming that the entire back of the mirror needs to be corrected by the magnetic write head; the duration of the correction process is  $T_{tot}$ . A first estimation of  $T_{tot}$  can be obtained using  $T_{tot} \approx S_{tot}/S_{mag} \times T_{mag}$ , where  $S_{tot}$  is the total surface area of the mirror,  $S_{mag}$  is the surface of the magnet and  $T_{mag}$  is the time spent for correcting  $S_{mag}$ . However, this calculation is not realistic enough, it does not take into account several phenomena, such as the fact that the magnet needs time to be recharged, or the limitation of the number of battery cycles per day. Hence, a more comprehensive calculation has been done to have a better estimation of  $T_{tot}$ . For comparison purposes, the baseline used for the calculation is that of JWST but with a diameter of 16 m. The influence of different variables is studied by varying one parameter at a time. The list of the

parameters that are used, along with their nominal value, can be found in Table 3.1 on page 35. At the beginning of each calculation, each parameter is set equal to its baseline value except for the variable that is under study. Then the time needed to change the shape of the mirror is calculated assuming that the time required to correct a given surface area is fixed, there is no feedback nor control. The limited size of the batteries and the power produced by the solar panels are taken into account during the computation.

### 3.3. Baseline Values of the Parameters

This section justifies and clarifies the baseline values that have been chosen for the different variables.

#### Size of the solar arrays

For the solar arrays, the JWST will have approximately  $26m^2$  of solar panels<sup>1</sup> but we choose to use an optimistic version of the JWST with photovoltaic panels of  $31 m^2$ .

#### Input power of the solar panels

To compute the input power of the solar arrays we use two methods. First we use radiation theory assuming that APERTURE, like JWST, is located at the Sun-Earth Lagrangian point L2 on a Lissajous orbit with a semi-major axis of 800,000 km [17]. This Lissajous orbit is approximated by a circular orbit with a radius equal to its semi-major axis. The Sun is considered to be a black body with a temperature of  $T_{Sun} = 5778K$ . The total power emitted by the Sun is computed according to Equation 3.1. The solid angle  $\Omega$  under which the telescope sees the Sun is computed from to Equation 3.2, where  $h$  is the radius of the orbit and  $d$  is the distance between the Sun and L2,  $d \approx 1.515 \times 10^8$  km. Then the power received by the solar panels is equal to the total power emitted by the Sun times  $\Omega/4\pi$ , the percentage received by the telescope (Equation 3.4).

$$P_{Sun,tot} = 4\pi R_{Sun}^2 \sigma T_{Sun}^4 \tag{3.1}$$

---

<sup>1</sup><http://jwst.nasa.gov/bus.html>

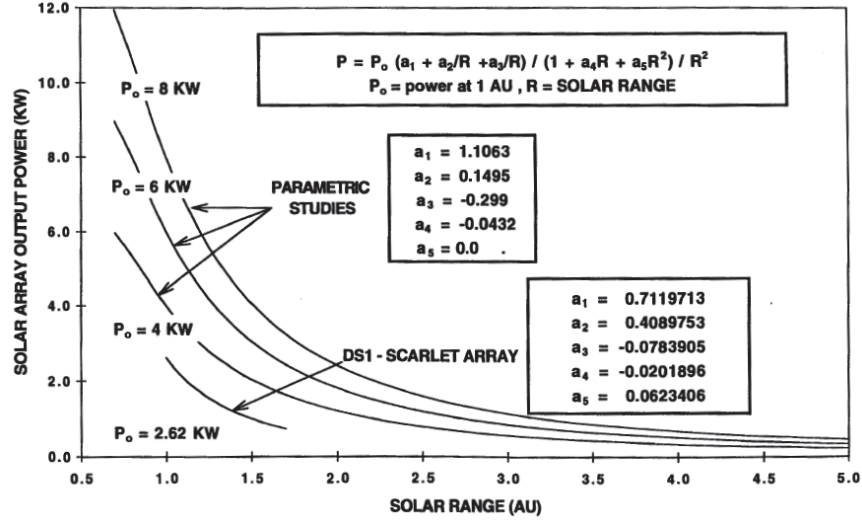


Figure 3.1: Solar array output power versus solar range using polynomials method [18]

$$\Omega = \frac{A_{Arrays}}{d^2 + h^2} \quad (3.2)$$

$$P_{Received} = \frac{\Omega}{4\pi} P_{Sun,tot} \quad (3.3)$$

$$= \sigma T_{Sun}^4 A_{Arrays} \frac{R_{Sun}^2}{d^2 + h^2} \quad (3.4)$$

The photovoltaic cells that are used are GaAs cells with an efficiency of 18% [19]. The result using this method is  $P_{Received} = 7431.44$  W. In order to confirm this result, we compare it to the polynomials method used in [18] and illustrated on Figure 3.1, with  $P_0 = 1358$  W/m<sup>2</sup>. We found  $P_{received} = 7442.82$  W, which is very close to the value we computed.

### Mission lifetime

The nominal value of the mission lifetime is set equal to the maximal lifetime of JWST, which is 10 years [17].

### Spacecraft main battery

JWST will use a 37 Ah NiH2 battery and the nominal mission operating voltage is

predicted to be between 30 and 32 V [17]. Hence, we take an average voltage of 31 V to calculate the size of the battery which is  $37 \times 31 \times 3600 \approx 4 \times 10^6$  J. The efficiency of the battery is 85%; note that this efficiency should decrease during the mission but it is taken constant to simplify the calculation. The depth of discharge (DOD) of the battery is 35%, like JWST [17]. This allows us to calculate the number of cycles per day using the method described on page 404 in [19] (see section 3.4.1). Using 10 cycles per day along with a mission lifetime of 10 years we find  $DOD = 39\%$  which is very close to the value indicated for JWST.

#### Percentage of the main battery allocated to charge the magnet

In order to estimate the percentage of the battery that will be allocated to charge the magnet in the APERTURE concept, we need to determine how much energy is required for other subsystems like the communication system. According to [20], JWST requires a communication time of 8 hours per day. We were not able to find exact specifications of JWST communication system but considering the DOD, the number of cycles per day and the duration of communication, we estimate the percentage of the battery that is allocated to the communication subsystem, is  $\approx 4.9\%$ . Now, based on the work done at Northwestern University about magnetic write heads we know that the magnetic write head requires a few Watts to work, hence we set the power required by the magnetic write head equal to 5 W. This value will need to be refined for future work and will be precisely measured during Phase II. Assuming that the magnetic write head is used all the time, we calculate that we can allocate about 1.7% to charge the magnetic write head. This leaves 93.4% for the other subsystems like the attitude determination and controls or the scientific instruments. This of course is a very simplified configuration, but it will give us an estimate of the time required to correct the mirror.

#### Size of the magnet battery

For the magnetic write head battery we assume a baseline size of  $2 \times 10^5$  J which corresponds approximately to a laptop battery. Using [19] we compute a DOD of about 49% for the given mission lifetime and this corresponds to a baseline value of about 4

cycles per day for the magnet battery.

### Number and size of the magnets

Finally, for the baseline case we assume we only have one magnet and that it covers an area of about  $1 \text{ cm}^2$  during a time of 3 s. Those two values give an order of magnitude of what we expect those parameters to be, but they will be accurately quantified during Phase II; they depend on cost and manufacturing issues along with the duration of the shape assessment process and other variables.

## 3.4. Results

### 3.4.1. Impact of Different Parameters

#### Diameter of the Primary Mirror

As expected,  $T_{tot}$  increases with the diameter of the mirror; more precisely it is a linear function of the diameter squared (Figure 3.2). This parameter has a large impact on the duration of the figure correction process. It is not a free parameter of the design given that the baseline for the APERTURE concept is a 16-m diameter primary mirror, but this analysis shows that the size of the telescope is not only limited by the rocket fairing but also by the time required to correct a very large mirror.

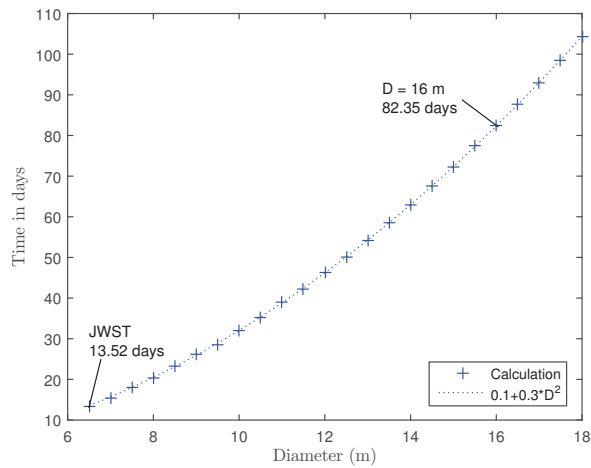


Figure 3.2: Time spent to correct the entire membrane as a function of the mirror's diameter.

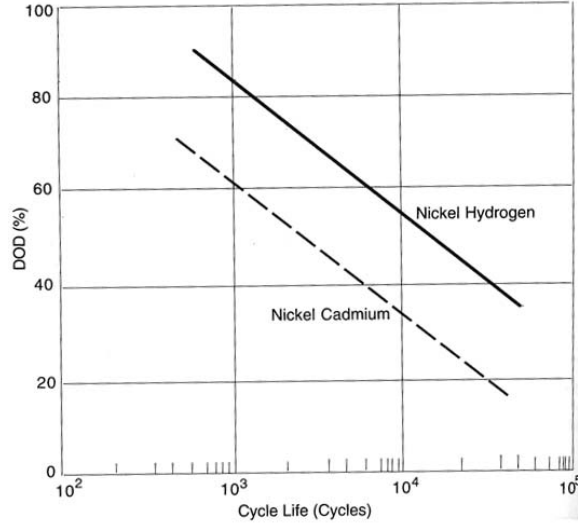


Figure 3.3: Depth-of-discharge versus cycle life for secondary batteries [19]

### Mission Lifetime

The mission lifetime drives the depth of discharge (DOD) of the spacecraft and of the magnet battery; when the mission lifetime increases, the DOD decreases according to Equation 3.5 which we derived from Figure 3.3 found in [19]:

$$DOD(\%) = -12.1602 \times \ln(NbCycles) + 166.9983 \quad (3.5)$$

Here  $NbCycles$  is the total number of cycles of the battery during the mission. Equation 3.5 corresponds to Nickel Cadmium batteries. To study the impact of this variable, the number of cycles per day has been taken constant. As shown on Figure 3.4,  $T_{tot}$  increases with the mission lifetime but, in order to maximize the mission goals, we preferred to keep the mission lifetime fixed, equal to JWST maximal lifetime, that is to say 10 years.

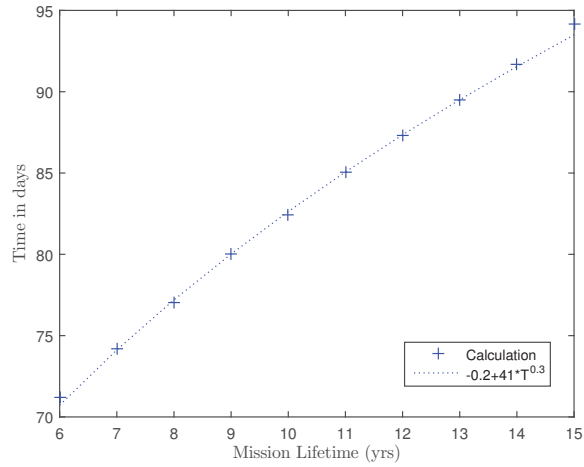


Figure 3.4: Time spent to correct the entire membrane as a function of the mission lifetime.

#### Number of Daily Cycles of the Magnet Battery

To study the impact of the number of daily cycles of the magnet battery, we take the mission lifetime equal to its baseline value, but the DOD can vary. As it is illustrated on Figure 3.5, this parameter does not have a huge impact on  $T_{tot}$  since it stays between 82.3 and 82.5 days over the entire range. Hence, this parameter is not crucial and does not drive  $T_{tot}$ .

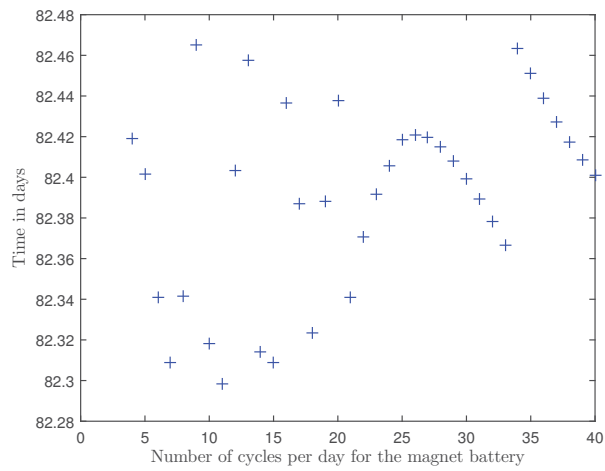


Figure 3.5: Time spent to correct the entire membrane as a function of the number of daily cycles of the magnet battery.



### Number of Daily Cycles of the Main Battery

Similarly, we take the mission lifetime equal to its baseline value but the DOD can vary. As one can see on Figure 3.6,  $T_{tot}$  decreases with the number of cycles of the main battery until a threshold value,  $\approx 20$  cycles/day, at which  $T_{tot}$  becomes constant. This change of  $T_{tot}$  behavior can be explained by the limited size and performance of the magnet battery: allowing the battery to recharge a large number of times per day is not necessary; there is a point at which the performance of the magnet battery becomes the limiting factor.

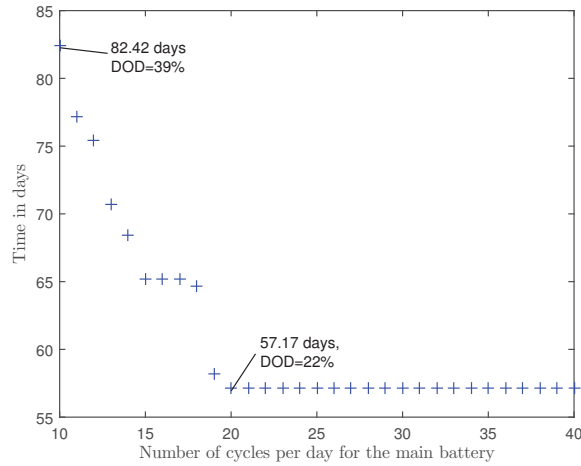


Figure 3.6: Time spent to correct the entire membrane as a function of the number of daily cycles of the main battery.

### Percentage of the main Battery Allocated to charge the Magnet

Figure 3.7 shows that  $T_{tot}$  decreases when a larger part of the main battery is allocated to charge the magnet, until a certain value,  $\approx 2.8\%$ , after which  $T_{tot}$  stays constant. This large change of  $T_{tot}$  behavior can be explained by the limited size of the magnet battery. Hence, it is not necessary to take a percentage greater than 3%. This value may change for different baseline values of the parameters.

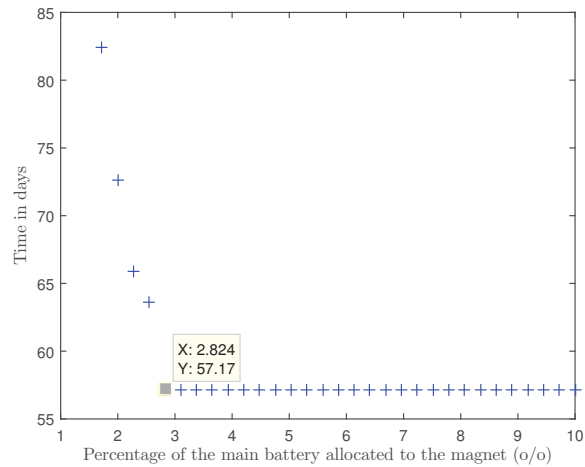


Figure 3.7: Time spent to correct the entire membrane as a function of the percentage of the main battery allocated to the magnet.

### Size of the Magnet Battery

The size of the magnet battery has a huge impact on the time required to correct the shape of the mirror. However, Figure 3.8 displays a horizontal asymptote. Hence, it is not really worth it to take a battery that is larger than the maximal value displayed on Figure 3.8, which has the same characteristics as a laptop battery.

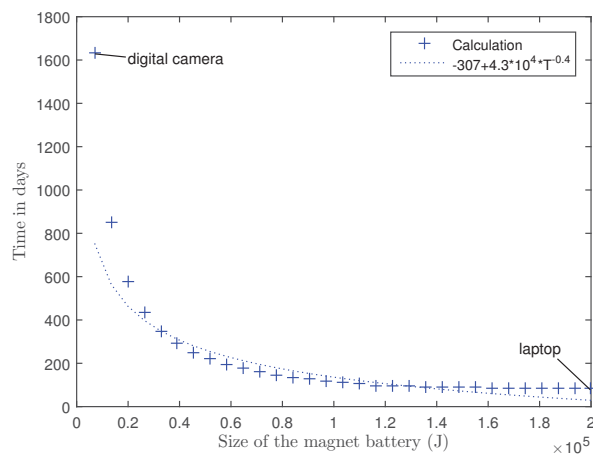


Figure 3.8: Time spent to correct the entire membrane as a function of the size of the magnet battery.

## Size of the Solar Panels

The size of the solar arrays has a very small impact on  $T_{tot}$  as one can see on Figure 3.9. This variable changes the time requires to charge the spacecraft main battery. It can be compared to the size of the solar panels for Hubble<sup>2</sup>, which has two panels of  $2.45 \times 7.56$  m, and to Rosetta<sup>3</sup>, which has  $64$   $m^2$ . Since it is not a driving factor, the area of the solar panels can be taken equal its baseline value.

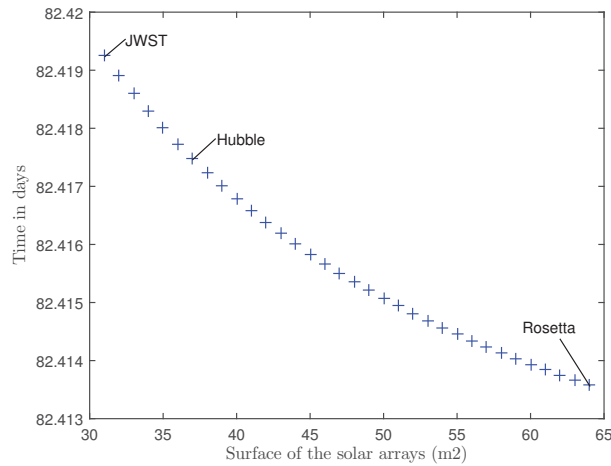


Figure 3.9: Time spent to correct the entire membrane as a function of the size of the solar panels.

## Surface of the Magnet

As illustrated on Figure 3.10 and as expected, the time necessary to correct the shape of the mirror decreases with the surface of the magnet, but the larger the magnet is, the closer to zero the slope gets. Note that this parameter is not totally free, it depends on the difficulties in manufacturing large magnetic write heads, and is limited by the minimal accuracy than one needs to control the parabolic shape. Hence, the value chosen for the preliminary design is likely to be modified but it is a credible estimation of the final value.

<sup>2</sup>[www.spacetelescope.org/about/general/fact\\_sheet/](http://www.spacetelescope.org/about/general/fact_sheet/)

<sup>3</sup>[www.esa.int/Our\\_Activities/Space\\_Science/Rosetta/Frequently\\_asked\\_questions](http://www.esa.int/Our_Activities/Space_Science/Rosetta/Frequently_asked_questions)

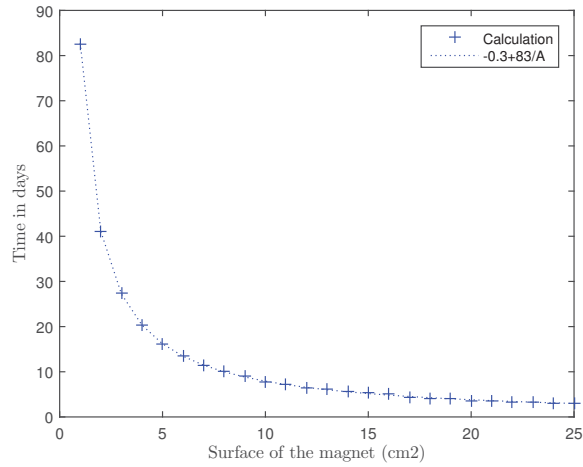


Figure 3.10: Time spent to correct the entire membrane as a function of the surface corrected by the magnet.

#### Time Allocated to Each Location

$T_{tot}$  increases linearly with the time spent to correct each point or "pixel" of the mirror, with a slope of 28 days/s. Similarly to the size of the magnetic write head, this variable cannot be chosen freely. It depends on the reaction time of the magnetic smart material, on the shape assessment duration, and on the convergence speed of the corrections.

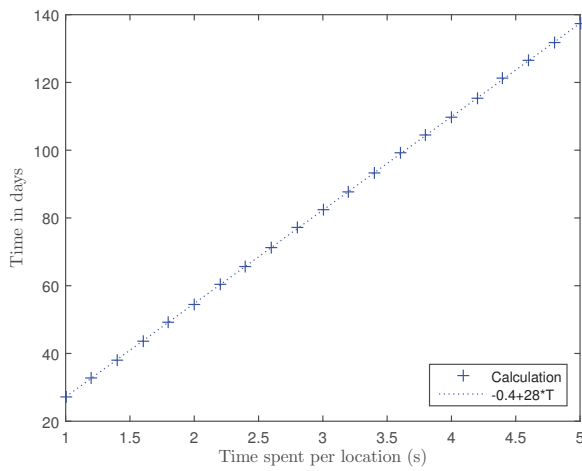


Figure 3.11: Time spent to correct the entire membrane as a function of the time allocated to each points that needs to be corrected.

## Number of Magnets

The number of magnets has a high impact on the time required to correct the primary mirror. However, the curve displays a horizontal asymptote (see Figure 3.12). Hence, after a certain value, the benefits of adding more magnets, which are a diminution of both  $T_{tot}$  and the failure risk thanks to redundancy, do not compensate the consequent drawbacks, which are the increased mass and complexity. For the preliminary design, 8 magnetic write heads are used.

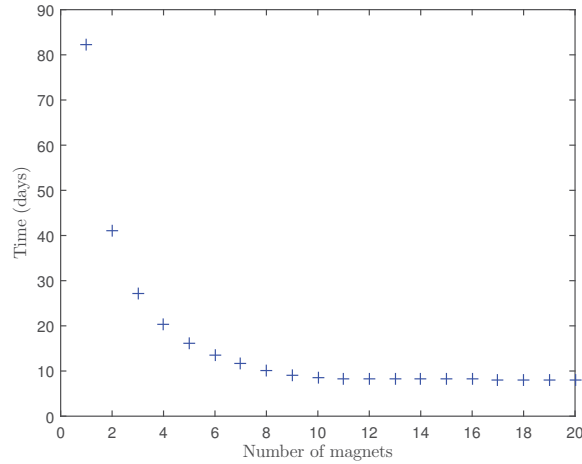


Figure 3.12: Time spent to correct the entire membrane as a function of the number of magnets.

### 3.4.2. Summary

Table 3.1 on page 35 shows a summary of the study described above. The influence of each variable can also be quantified by the percentage of impact detailed in Equation.

$$P_j = \frac{\Delta T_j}{\sum_i \Delta T_i} \frac{V_j}{\Delta V_j} \quad (3.6)$$

Here  $V_j$  is the baseline value given to the parameter, indexed by  $j$ , when another variable is studied,  $\Delta V_j$  gives the range of values taken by the parameter when its impact is computed,  $\Delta T_j$  is the difference between the maximal and minimal  $T_{tot}$ .

The result is shown in Figure 3.13. As one can see, using this definition of the percent-

age of impact, the most significant parameter is the size of the magnet battery. Thus, the time required to correct the shape of the primary in this worst-case scenario can be greatly improved if the design and manufacturing constraints allow for larger magnetic write head batteries. In order to compare the impact of the other studied variables, Figure 3.14 has been obtained by removing the data corresponding to the magnet's battery. Once setting the diameter of the mirror equal to a certain value, one can use the most significant parameters, which are the size of the magnet's battery, the time allocated to each point, the mission lifetime, the number of daily cycles for the main battery, the number of magnets, and the surface of the magnet, in order to create an optimal design and meet the requirement in terms of time spent to correct the shape of the membrane. This analysis enabled us to identify the most important variables that we will need to take into account to create the optimal design for APERTURE.

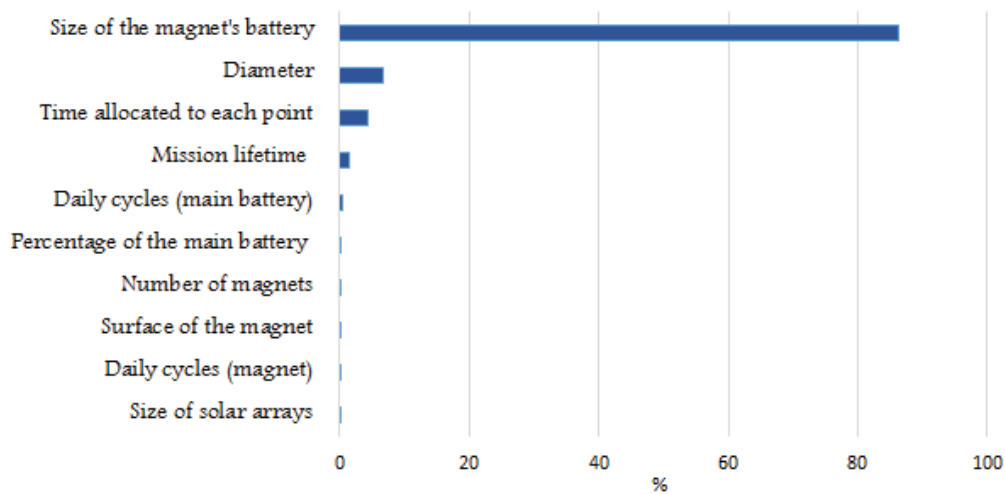


Figure 3.13: Quantification of the impact of different parameters on the time needed to correct the entire mirror, see Equation 3.6 (with all parameters included)

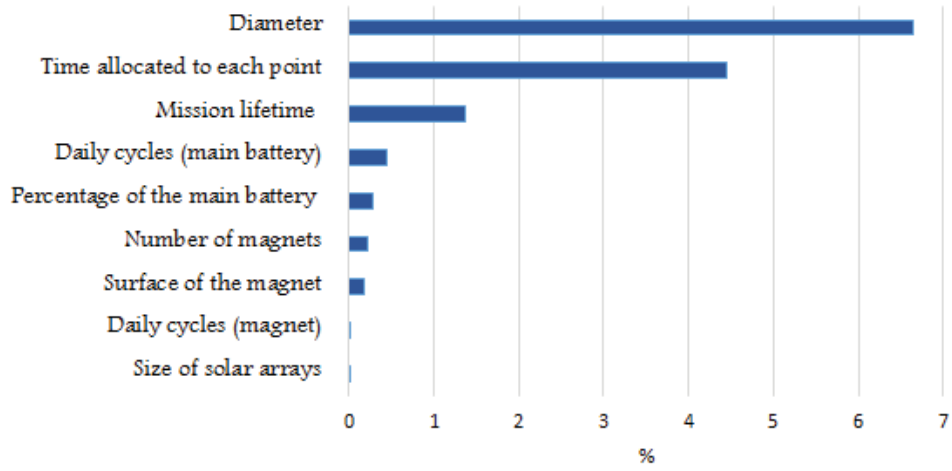


Figure 3.14: Quantification of the impact of different parameters on the time needed to correct the entire mirror, see Equation 3.6 (without the size of the magnet battery)

Parameter	Range	Nominal Value	Constraints	Impact	Horizontal Asymptote	Preliminary design
Diameter	6.25 - 18 m	16 m	Rocket fairing	High	No	16 m
Mission lifetime	6 - 15 yrs	10 yrs	Mission goals, Battery performances	Moderate	No	10 yrs
Daily cycles (magnet)	4 - 40 cycles/day	4 cycles/day	Battery Performances	Very Low	No	11 cycles/day
Daily cycles (main battery)	10 - 40 cycles/day	10 cycles/day	Battery Performances	Moderate	Yes	20 cycles/day
Percentage of the main battery used to charge the magnet battery	1.72 - 10 %	1.72 %	Other subsystems requirements (communication, instruments...)	Moderate	Yes	3%
Size of the magnet's battery	7.E3 J (digital camera) - 2.E5 (laptop) J	2.E5 J	Mass requirement, Performances of the arm holding the magnet	Very High	Yes	2.E5 J
Size of solar arrays	31 m <sup>2</sup> (JWST) - 37 m <sup>2</sup> (Hubble) - 64 (Rosetta) m <sup>2</sup>	31 m <sup>2</sup>	Rocket Performances (mass) and Dimensions	Very Low	Yes for large values	31 m <sup>2</sup>
Surface of the magnet	1 - 25 cm <sup>2</sup>	1 cm <sup>2</sup>	Manufacturing Limitations	High	Yes	2 cm <sup>2</sup>
Duration to treat each location	1 - 5 s	3 s	Magnetostriction properties, shape assessment duration	High	No	3 s
Number of magnets	1-20	1	Mass requirement	High	Yes	8 magnets
					Total time	3.68 days

Table 3.1: Summary of the impact of different parameters over the time required to correct the mirror.



## CHAPTER 4 PRELIMINARY APERTURE DESIGN

### 4.1. Magnetic Smart Material and Substrate

There are a wide range of MSMs available. For simplicity we choose the strongest one, Terfenol-D, but Phase II funding would allow us to explore the approach of using a material that has both strong enough magnetostriction and high remanence, such as Vanadium-Permadrur. Based on initial deflection studies on glass with an approximate 0.1 T field and a 4  $\mu\text{m}$  Terfenol-D film, we will baseline a 4  $\mu\text{m}$  Terfenol-D film, and  $< 1 \mu\text{m}$  NiCo film or FeCo film to hold in the magnetic field. The substrate could be as thin as 5  $\mu\text{m}$  made up of a polyimide such as Kapton or CP-1. An alternative approach would be to use some shape memory composite whose front surface could be shiny electro-formed material such as Ni which is known to have a deployed shape good enough for the microwave regime [21].

### 4.2. Magnetic Write-Head

The very tentative design would be a horseshoe geometry of soft magnetic material such as iron with a gap separation of 3 mm to 1 cm or even larger. With larger spacing, a stronger current and more windings would be needed, but conversely, the larger (within reason, i.e. no more than  $\sim 10\text{cm}$ ) the size of the “pixels” of the mirror that can be corrected, the better. It is true because a larger pixel size means fewer total pixels that will need correction. If the power requirement becomes too great, the fall back is to use permanent magnets whose gap strength can be controlled mechanically. We give an example of each type of design in Figure 4.1.

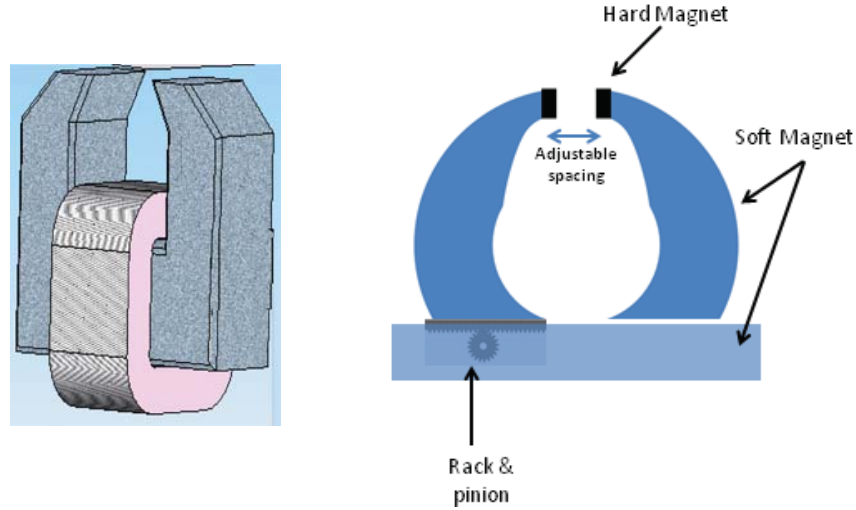


Figure 4.1: In both cases the magnets have been designed so that the magnetic field runs primarily parallel to the surface. Left: Simplified drawing of an electromagnet provided by Dr. C. Joshi of Altranex Corp. Ontario, Canada. Right: Schematic of a permanent magnet design whose effective magnetic field strength can be adjusted, courtesy of Drs. C. S. Arnold and D. Pappas of NIST Boulder, Colorado, USA

#### 4.3. Stowed Configuration and Deployment Mechanism

The primary mirror membrane can be stowed in a Delta IV Heavy rocket fairing using the umbrella design introduced in section 2.2. The preliminary design assumes a focal length equal to the diameter of the primary mirror. The secondary mirror and the inner hole of the primary mirror have a diameter of 4.5 m, which corresponds to the utilization of 92% of the available light-collecting surface area. The height of the stowed membrane is about 8 m while its diameter is 3.9 m. This design exhibits very low local radii of curvature, the minimum being 1 mm. Hence, to avoid any risk of micro-yield, if aluminum is used as the reflective layer, Kapton as the substrate and Galfenol as the magnetostrictive material, they have to be less than  $8 \mu\text{m}$ ,  $7 \mu\text{m}$  and  $9 \mu\text{m}$  respectively (see section 2.4.2). This may not be the final composition of the membrane but the same method can be applied to other materials once they are selected. The deployment of the umbrella membrane will be based on the flexible reflector which uses a memory composite material, leading to a slow and controlled deployment. An alternative design is the self-deployable shell reflector which can be used for reflectors up to 17-m given the height of the Delta IV Heavy rocket fairing,

while the umbrella design could be scaled-up. In all cases, the RMS figure accuracy will need to be improved from its deployed value in order to be effective for the UV-Vis wavelength range.

#### 4.4. Post-Deployment Figure Assessment and Feedback

Two designs have been selected from a literature survey. The first design is that being used for JWST [22] which involves determining where a reference star is imaged from each segment in an out of focus image. Then, each segment is adjusted via a tip-tilt and push-pull until each star image is at its proper location. In the second approach, a standard Shack-Hartmann test is used to adjust the figure [23].

#### 4.5. Operations of the In-Space Shape Correcting System

The estimation of the time required to correct an entire 16-m mirror, with a single magnetic write head, and using the baseline values of Table 3.1 on page 35, is about 82 days, but this number can be reduced by adding magnetic write heads and changing the other significant variables. An example of a modified design is proposed in Table 4.1 and corresponds to a total time of only **3.7 days**. When the shape assessment, feedback process and parameters of the magnetic write heads are known in details, the various design parameters used in chapter 3 can be computed to obtain an optimal and feasible design for operation management.

Table 4.1: Alternative design, reduced total time

Diameter	16 m
Mission lifetime	10 yrs
Daily cycles (magnet)	11 cycles/day
Daily cycles (main battery)	20 cycles/day
Percentage of the main battery used to charge the magnet battery	3%
Size of the magnet's battery	$2 \times 10^5$ J
Size of the solar panels	31 m <sup>2</sup>
Surface of the magnet	2 cm <sup>2</sup>
Time allocated to each point	3 s
Number of magnets	8
Total time	3.7 days

## CHAPTER 5 CONCLUSION

In summary, astronomical as well as Earth observing applications of the future are counting on larger aperture telescopes than are currently available. Several groups have been working on the topic of enabling large (about 16-m diameter) UV-Vis telescopes for many years. The unique feature of the APERTURE concept is that magnetic films are used rather than electrostatic films or piezo-electrostatic pads. The preliminary work that has been described in this report about the stowing, deployment and post-deployment shape corrections feasibility has been very conclusive. Nevertheless, there are still several unknowns related to the initial accuracy of the deployed figure prior to the magnetic write head corrections. The length scale over which the corrections need to be applied is also of concern. However, deployment strategies and the materials available continue to evolve, in particular shape memory composites (SMCs) [21] or alloys (SMAs) [24], such that at this time we see no show-stoppers for this concept. Furthermore, the ability to tune deformations down to much (factors of 10-100) smaller ( $\sim \mu\text{m}$ ) scale opens the futuristic possibility of improving the figure well beyond Strehl values of 90%.

### 5.1. Future Work

#### 5.1.1. Concept Verification Testing

Several tests are proposed to validate the main concepts of the APERTURE system including MSM mirror reflection and deployment tests. This study dealing with the future test campaign for APERTURE has been carried out by several members of the team at UIUC.

The Shack-Hartmann wavefront sensor test is an optical method for determining the wavefront shape of a parabolic mirror. Shack-Hartmann sensors provide accurate wavefront shape feedback via measurement of the localized slope of the wavefront error. This measurement is performed using a lenslet array to split the incoming wavefront into an array of smaller beams. Each beam is focused onto a CMOS camera placed on the focal plane of the lenslet array [25]. Each lenslet creates a spot along the optical axis which can be used to calculate the local wavefront tilt across each lens.

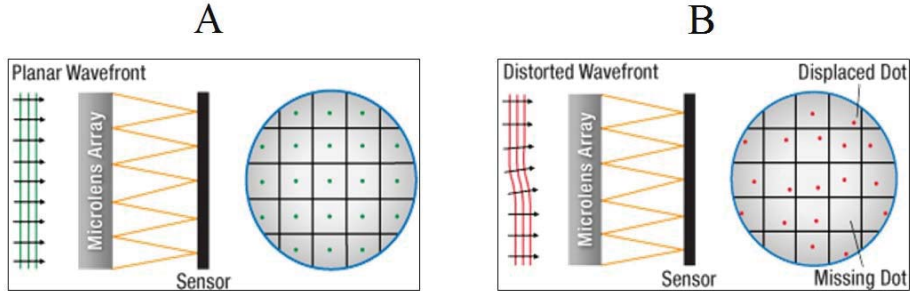


Figure 5.1: (A) Image of a regularly spaced grid. (B) Image of a grid from a distorted wavefront [25].

A non-distorted wavefront creates a regularly spaced grid of spots, while a distorted wavefront causes some lenslets to displace their corresponding spots and create an irregular grid. Therefore, the whole wavefront shape can be determined from the grid spots provided by the lenslet array. Figure 5.1 illustrates the figure when the shape is correct (A) and when it needs correction (B).

A Shack-Hartmann test implements a simple setup for the testing of optical lenses and mirrors. It consists of a point source, Shack-Hartmann wavefront sensor, laser collimating lens, beam reducer, beam splitter, illuminating lens, and a reference lens. Table 5.1 identifies these components along with their characteristics. Figure 5.2 shows the setup geometry of the test components for the testing of the reference lens, as determined by the National Institute of Standards and Technology [26]. For the purposes of validating an MSM reflective mirror, the test will be performed vertically instead of the traditional horizontal setups. This allows the gravity to aid the MSM membrane to maintain its curved shape. The location of the components relative to each other is a function of the focal length of the mirror. A laser diode in the visual spectrum will be the point source for this experiment. The illuminating lens is sized to guarantee both the reflected light of the mirror and the laser diode cover their respective targets. This size is a simple function of the focal length as well as the wavefront sensor aperture size.  $S_o$  and  $S_i$  represent the distances between the Beam Reducer and Illuminating Lens and between the Illuminating Lens and the Object Under Test, respectively. They were found to be 27.5 cm and 2.75 cm using equations (5) and (6).

Table 5.1: Shack-Hartmann Test Components

Component	Manufacturer and Part Number	Characteristics
Wavefront sensor	Thorlabs WFS300-14AR	300 $\mu\text{m}$ Pitch, AR Coated: 400-900 nm
Beam Reducer	Thorlabs GBE03-A	3X Expander, AR Coated: 400-650 nm
Beam Splitter	Thorlabs BS025 - 10:90 (R:T)	Non-Polarizing Cube 400-700 nm, 1"
Illuminating lens	Thorlabs LA1560-D	12.7 mm Diameter, 25 mm Focal Length
Reference Lens	Newport Concave Lens	50.8 mm Mirror, 250mm EFL

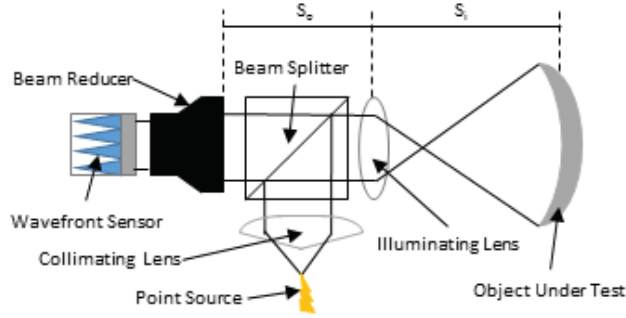


Figure 5.2: Test Geometry for Shack-Hartmann

$$S_o = f_1 + f_t \quad (5.1)$$

$$S_i = \frac{f_1^2 + f_t f_1}{f_t} \quad (5.2)$$

As mentioned above, a deployment verification test will need to be performed. The purpose of this test is to show that the aforementioned deployment method will unfurl the membrane without it ripping or catching. A scale model test could be performed in one of two ways, using the deployment mechanisms selected in section 2.5. Both ways would use an analog material to the MSM membrane to reduce test cost. The first method would be a powered test using powered actuators. The other option is an empowered test using springs. The exact details of this test will be worked out at the initial portion of Phase II.

### 5.1.2. Tall Poles for Phase II

Even though no showstoppers have been found during Phase I, the team has identified possible obstacles and questions that remain for the APERTURE Concept. In order of precedence:

1. Can we get any membrane-like material to deform in a controlled manner and have the shape remain for days to weeks, minimum?
2. Can the two selected deployment mechanisms produce a near net shape to about 300-400  $\mu\text{m}$  that will have such a low in-plane stress that further correction via magnetostriction is possible?
3. Can the deployed membrane be such that any required corrections are on length scales greater than 1 cm, as correcting mm length scale errors would be extremely challenging?
4. Is a closed-loop controller possible for in-orbit figure assessment and correction?
5. Are the disparities in the materials' Coefficients of Thermal Expansion (CTE) critical for the shape correction process? Is thermal control necessary, in particular because of shape memory composite?
6. Can pieces of membrane be stitched together as it would be technically challenging to coat a monolithic 16-m (or larger) diameter mirror?
7. Can the position of the magnet be accurately determined and controlled, both in distance from the substrate and in radius and azimuth relative to the optical axis?
8. Is a secondary deformable mirror a credible path given that, the smaller the deformable mirror, the smaller the resulting field of view?
9. Instead of being placed at the L2 point, can APERTURE be used in GEO?

Question 1 was partially answered during Phase 1 but it needs more in-depth investigation, especially about the in-plane stretch. The membrane boundary may need active control which could also counteract the elastomer creep produced under

UV exposure. This first topic will be investigated through Tasks 1 and 2, which will also address item 4. Questions 2 and 3 are very challenging since deployed membranes tend to have systematic-type errors and low spatial frequency errors that are hard to eliminate. Those issues will be tackled with Task 3. Question 5 about thermal control has not been addressed during Phase I, and time may not permit to investigate this topic but the team will complete the different tasks of Phase II keeping in mind that thermal control may be critical. For instance, while choosing the materials in Task 1.1, the CTEs will be taken into account. Temperature can be controlled thanks to a sun shield, a material combination that offers minimal mechanical response under thermal gradients, or by an active system. Some of the other questions may be addressed in Task 5 if time permits.

### 5.1.3. Work Plan for Phase II

During Phase I, no show stoppers were found, albeit we are far from a final working proof of concept. Thus, continued study into the material selection for the MSM and substrate, deployment design and implementation, and magnetic write head design is required to confirm the viability of APERTURE. A Phase II effort will perform proof of concept experiments for the critical items of deployment and surface correction. Several  $5 \times 5$ -cm or  $10 \times 10$ -cm flat samples with different substrates and MSM coatings will be fabricated for testing plane rectification. The exact size will depend on the details of the coating process(es) used, .e.g. sputtering on  $5 \times 5$ -cm flat sample is straight forward as is electroplating  $10 \times 10$ -cm pieces. Also, several stowed prototypes will be created to explore deployment strategies. Along with the experiments, detailed numerical modeling and simulations will be performed.

The *Herschel* telescope worked in the range about 50-700  $\mu\text{m}$  and had a diameter of 3.6 m [27]. Thus a first step in our development would be to achieve diffraction limit in this waveband. This is longer than UV-Vis wavelength by about 100-1,000, but such a telescope could be a pathfinder. The caveat of such an approach is that the sub-mm mirrors like *Herschel* need to be cooled to 85K, and then CTE mismatch between the coating and the substrate could lead to distortions that are beyond the ability of our



design to correct. There is an alternative strategy in image correction: suppose that after correcting the primary figure, further image improvements are needed. Then the image could be further improved via a deformable secondary mirror (DM) [28]. The secondary could be of the classic design used to correct for atmospheric turbulence in ground-based adaptive optics systems. The down side of a DM is that the smaller it is relative to the primary, the smaller the effective field of view (FOV). There is a simple rule of thumb is that the FOV decreases as the ratio of the diameter of the DM to the primary so that, for a 20 cm diameter DM and a 16m diameter primary, if the FOV of the primary is 1 degree, the resulting FOV of the primary plus DM is about 45".

Below is a detailed breakdown of the tasks.

### **Task 1: Analysis of MSM Coated Flat Membrane (6 months-NU)**

One of the major tasks for Phase II is to demonstrate experimentally that we can apply a controlled deformation of a MSM coated membrane using magnetostriction. The goal will be to create deformations up to the order of 300  $\mu\text{m}$  and to demonstrate that the deformation remains constant on the level of a 1  $\mu\text{m}$  over at least 1 week. First, a flat membrane will be used and, if time permits, a curved sample will be produced to measure the focusing ability of the corrected membrane. The substrate used for this test will be the low cost polyimide film  $\text{\textcircled{R}}$ Kapton which can be molded to make a curved sample. If time permits, other optional substrates will be investigated.

#### Task 1.1: Decision about MSM Choice (2 months)

During Phase I two types of MSM have been selected; this choice will be refined and finalized to determine which magnetostrictive material will coat the samples. The amount of magnetostriction that is needed will be determined as part of this study.

#### Task 1.2: Production of Test Samples (1 month)

At least two samples of 5x5 cm will be made for each type of MSM in order to test the repeatability of the experiment. The simplest approach to deposit the MSM on the substrate is to use the system that is currently used at NU, which can sputter

Terfenol-D and coat pieces that are 5 cm square. An alternative to this method is electroplating, but this option is too expensive for the team's budget.

### Task 1.3: Evaluation of Test samples (3 months)

The sample will be mounted such that there is low in-plane stress. For instance, it can be clamped on all sides. Then it will be placed in a magnetic field (generated by permanent magnets or an electromagnet, or both in separate tests) that would cause a controlled deformation. Both the magnetic field and the surface shape will be measured. For the curved sample, a Shack-Hartmann test will be used to measure the accuracy of the optical figure. Due to the different CTEs of the materials, the samples will need to be put in a controlled thermal environment. The team is considering using a glove box equipped with a thermal control system. One unknown after Phase I is the time during which the membrane can hold the shape induced by magnetostriction. After being exposed to the magnetic field, the sample will be put at rest and its shape will be measured after 1.5, 5, and 7 days. This test can be repeated as needed.

### **Task 2: Simulation of Membrane Shape Correction Using Magnetostriction (1 year-NU)**

The team needs to show that the deformations produced the magnetic field applied on the MSM can converge to the desired shape for the membrane and eventually to an improved reflected image.

### Task 2.1: Investigation of Feedback Loop Controller (8 months)

The team will develop the ability to cause deformations in specific locations on the flat membrane in a non-interfering manner. In other words demonstrate that deformations at locations (call them A and B) about 1 cm apart can be produced such that the net deformations at A and B both have the desired value. To carry out this task the team can use deformable mirror software <sup>1 2 3</sup> along with measurements made via lasers positioning systems such as <sup>4</sup> or as in an adaptive optics laboratory demonstration kit

---

<sup>1</sup>[www.mathworks.com/matlabcentral/fileexchange/33330-zernikecalc?s\\_tid=srchtitle](http://www.mathworks.com/matlabcentral/fileexchange/33330-zernikecalc?s_tid=srchtitle)

<sup>2</sup>[www.openchannelsoftware.com/projects/PROPER](http://www.openchannelsoftware.com/projects/PROPER)

<sup>3</sup>[www.okotech.com/mrfit](http://www.okotech.com/mrfit)

<sup>4</sup>[resources.renishaw.com/en/details/data-sheet-rle-system-performance--33411](http://resources.renishaw.com/en/details/data-sheet-rle-system-performance--33411)

for deformable optics such at ThorLabs<sup>5</sup> in order to demonstrate that the figure can be improved using our approach.

#### Task 2.2: Simulation of Image Improvement (4 months)

After simulating the modifications in the membrane induced by magnetostriction, the results of Task 2.1 can be translated in terms of resulting image accuracy. Two types of image simulations will be done: first, using the size of the deflections obtained during the experiments of Task 1, and, second, using half the maximal deflection that is necessary to correct the post-deployment RMS error. This task can be linked to Task 3.4 by determining the length scales of the corrections that must be produced versus deployment ability.

### **Task 3: Verification of Deployment Methodology (18 months-UIUC)**

Another major task of Phase II will be to demonstrate that the two deployment mechanisms selected during Phase I lead to a good enough post deployment surface accuracy. The aim is to prove that the RMS error of the deployed membrane can be corrected using magnetic write heads and magnetostriction. The target is to get an RMS error of about 100  $\mu\text{m}$ .

#### Task 3.1: Design of Deployment Ground Test (6 months)

The flexible reflector and the self-deployable shell selected during Phase I require two different deployment mechanisms. The first one is slowly controlled by heating an elastic memory composite, while, for the second design, the deployment lasts only 2 s. Hence, the team at UIUC will need to design two different procedures to test experimentally the deployment mechanisms. Another issue to tackle is how to measure the surface accuracy of the post-deployment shape of the membrane. An indirect method like the Shack-Hartmann test or photogrammetry techniques can be used to measure the surface shape before and after deployment.

#### Task 3.2: Fabrication of Deployment Structures (3 months)

Two models will be manufactured, one for each design. These models will be scaled

---

<sup>5</sup>[www.thorlabs.com/newgrouppage9.cfm?objectgroup\\_id=3208](http://www.thorlabs.com/newgrouppage9.cfm?objectgroup_id=3208)

down compared to the desired 16-m diameter APERTURE primary; and they will probably be about 30 cm to keep material costs low and to accommodate available lab space.

Task 3.3: Evaluation of Deployment Method (3 months)

After deploying the folded structures, the two deployments will be evaluated using the measured RMS error of the post-deployment shape. A cloth or thin film of nearly identical flexibility properties to the MSM covered membrane will be used as the primary mirror. This approach will be utilized to lower test cost and to allow the deployment tests to occur independently of the MSM coated membrane tests. The deployment test will be done several times in order to determine the repeatability of each approach.

Task 3.4: Analysis of Test Results (6 months)

The two deployment designs will be compared according to the following criteria: resulting RMS error, repeatability, stowed volume efficiency, stability, weight and cost.

**Task 4: Further Investigations and Design of Full-Concept Demonstrations (6 months-UIUC)**

Tasks 1-3 begin to answer the questions surrounding the APERTURE concept introduced earlier in this section. This information will enable the updating of the mission concept. However, further investigation will be required to fully answer the questions after Phase II. An on-orbit demonstration of the APERTURE concept presents the comprehensive next step in this effort.

Task 4.1: Refinement of Mission Concept (1 month)

Several steps will be undertaken to update the full mission concept. First, the utilization of a magnetic read and write head instead of just a write head will be considered. Two designs have been identified for the magnetic write head. Additionally, an updated concept of operations (ConOps) will be constructed using the results from Tasks 1, 2 and 3 and a selected concept for the magnetic write head system. A preliminary study will be done to compare the assets and drawbacks of in-orbit versus ground

demonstrations.

Task 4.2: Design of an On-Orbit or Ground Demonstration Mission (5 months)

Depending on the result of Task 4.1, the design of an on-orbit or a ground demonstration will be initiated. A CubeSat mission would provide a dedicated, independent, on-orbit platform for evaluating the concept. UIUC will leverage their considerable experience designing and constructing several flight CubeSats as well as performing CubeSat mission concept studies (including for JPL) to design a CubeSat scale APERTURE demonstration payload and its corresponding mission. The demonstration design concept will be matured to the degree that it could be enacted after Phase II.

**Task 5: Reporting and meeting**

Progress reports will be done every 3 months, the team will also participate to the midterm review and will deliver a final report along with annual key enabling technologies reports. The PI Prof. Ulmer will attend to the NIAC symposiums.

## CHAPTER 6 PUBLICATIONS AND CONFERENCES

In addition to the final report which is available as a NIAC report in the public domain, we submitted the following article:

- M. P. Ulmer, V. L. Coverstone, J. Cao, *et al.*, "APERTURE, a large telescope using magnetostriction for post deployment corrections, an update", *in Proc. SPIE Astronomical Telescopes + Instrumentation, in Edinburgh, UK, 26 June - 1 July 2016*

We plan to participate in the following conference by attending and by giving a oral presentation at:

- SPIE Astronomical Telescopes + Instrumentation, in Edinburgh, UK, 26 June - 1 July 2016.

## REFERENCES

- [1] M. Postman, T. Brown, K. Sembach, *et al.*, “Advanced Technology Large-Aperture Space Telescope: science drivers and technology developments,” *Optical Engineering* **51**, 011007–011007 (2012).
- [2] H. P. Stahl, H. Thronson, S. Langhoff, *et al.*, “Potential astrophysics science missions enabled by NASA’s planned Ares V,” in *UV/Optical/IR Space Telescopes: Innovative Technologies and Concepts IV, Society of Photo-Optical Instrumentation Engineers (SPIE) Conference Series* **7436**, 743607 (2009).
- [3] C. F. Lillie, R. S. Polidan, and D. R. Dailey, “Key enabling technologies for the next generation of space telescopes,” in *Space Telescopes and Instrumentation 2010: Optical, Infrared, and Millimeter Wave, Society of Photo-Optical Instrumentation Engineers (SPIE) Conference Series* **7731**, 773102 (2010).
- [4] “Three newly designed tracking and data relay satellites to help replenish existing on-orbit fleet,” Tech. Rep. FS-2001-9-025-GSFC, NASA Goddard Space Flight Center (2001).
- [5] M. W. Thomson, “Astromesh<sup>TM</sup> deployable reflectors for Ku-and Ka-band commercial satellites,” in *20th AIAA International Communication Satellite Systems Conference and Exhibit*, (2002).
- [6] J. R. Hill, K. W. Wang, H. Fang, *et al.*, “Actuator grouping optimization on flexible space reflectors,” in *Proceedings of SPIE - The International Society for Optical Engineering*, **7977** (2011).
- [7] “Replicated diffractive optics, moire.” <http://www.ballaerospace.com/page.jsp?page=259>. Accessed: 2015-01-26.
- [8] S. E. Kendrick, R. Linfield, and D. Ebbets, “Optical requirements for a Terrestrial Planet Finder optical coronagraph primary mirror,” in *Techniques and Instrumentation for Detection of Exoplanets*, D. R. Coulter, Ed., **5170**, 13–24 (2003).
- [9] “Delta IV, Payload Planners Guide,” tech. rep., United Launch Alliance (2007).

- [10] J. Enders, Kas-Danouche, W. Liao, *et al.*, “Design of a membrane aperture deployable structure,” in *44th AIAA/ASME/ASCE/AHS Structures, Structural Dynamics, and Materials Conference, AIAA Conf. Proc.*, (Norfolk, Virginia) (2003).
- [11] J. Domber and L. Peterson, “Implications of material microyield for gossamer optical reflectors,” in *43rd AIAA/ASME/ASCE/AHS/ASC Structures, Structural Dynamics, and Materials Conference*, American Institute of Aeronautics and Astronautics (AIAA) (2002).
- [12] J. H. Li, X. X. Gao, J. Zhu, *et al.*, “Ductility, texture and large magnetostriction of fe-ga-based sheets,” *Scripta Materialia* **63**(2), 246–249 (2010).
- [13] P. N. Keller, M. S. Lake, D. Codell, *et al.*, “Development of elastic memory composite stiffeners for a flexible precision reflector,” in *Collection of Technical Papers - AIAA/ASME/ASCE/AHS/ASC Structures, Structural Dynamics and Materials Conference*, **10**, 6984–6994 (2006).
- [14] O. Soykasap, S. Karakaya, and E. Kaplan, “Self-deploying composite shell reflector antenna for ku-band missions: 1.5 m diameter demonstrator,” in *RAST 2013 - Proceedings of 6th International Conference on Recent Advances in Space Technologies*, 631–636 (2013).
- [15] O. Soykasap, S. Karakaya, A. Gayretli, *et al.*, “Preliminary design of deployable flexible shell reflector of an x-band satellite payload,” in *2nd AIAA Spacecraft Structures Conference*, (2015).
- [16] K. Hearon, P. Singhal, J. Horn, *et al.*, “Porous Shape Memory Polymers,” *Polymer reviews (Philadelphia, Pa.)* **53**, 41–75 (2013).
- [17] P. Stanley, “JWST Mission Operations Concept Document,” tech. rep., Space Telescope Science Institute (2006).
- [18] S. N. Williams and V. Coverstone-Carroll, “Benefits of solar electric propulsion for the next generation of planetary exploration missions,” *Journal of the Astronautical Sciences* **45**(2), 143–159 (1997).



- [19] W. Larson and J. Wertz, *Space mission analysis and design*, Space technology library, Microcosm (1992).
- [20] J. Gal-Edd and E. Luers, “James webb space telescope ka-band trade,” (2004).
- [21] S. J. Varlese, M. P. Ulmer, J. Hermiller, *et al.*, “Performance characterization of a shape memory composite mirror,” in *UV/Optical/IR Space Telescopes: Innovative Technologies and Concepts II*, H. A. MacEwen, Ed., *Society of Photo-Optical Instrumentation Engineers (SPIE) Conference Series* **5899**, 331–339 (2005).
- [22] J. S. Knight, D. S. Acton, P. Lightsey, *et al.*, “Observatory alignment of the James Webb Space Telescope,” in *Space Telescopes and Instrumentation 2012: Optical, Infrared, and Millimeter Wave*, *Society of Photo-Optical Instrumentation Engineers (SPIE) Conference Series* **8442**, 84422C (2012).
- [23] M. B. Quadrelli, L. J. Wood, J. E. Riedel, *et al.*, “Guidance, Navigation, and Control Technology Assessment for Future Planetary Science Missions,” *Journal of Guidance Control Dynamics* **38**, 1165–1186 (2015).
- [24] S. Padula, S. Qiu, D. Gaydosh, *et al.*, “Effect of Upper-Cycle Temperature on the Load-Biased, Strain-Temperature Response of NiTi,” *Metallurgical and Materials Transactions A* **43**, 4610–4621 (2012).
- [25] *Optical wavefront Sensors (Shack-Hartmann)*, *WFS Series, Operation Manual* (2015).
- [26] D. R. Neal, P. Pulaski, T. D. Raymond, *et al.*, “Testing highly aberrated large optics with a shack-hartmann wavefront sensor,” in *Proceedings of SPIE - The International Society for Optical Engineering*, **5162**, 129–138 (2003).
- [27] G. L. Pilbratt, J. R. Riedinger, T. Passvogel, *et al.*, “Herschel space observatory: An esa facility for far-infrared and submillimetre astronomy,” *Astronomy and Astrophysics* **518** (2010).
- [28] “The adaptive secondary mirror for the vlt.” <http://www.eso.org/sci/facilities/develop/ao/sys/dsm.html>. Accessed: 2015-01-29.